

Identification of high-spin proton configurations in ^{136}Ba and ^{137}Ba

L. Kaya,^{1, a} A. Vogt,¹ P. Reiter,¹ C. Müller-Gatermann,¹ A. Gargano,² L. Coraggio,² N. Itaco,^{2, 3} A. Blazhev,¹ K. Arnsward,¹ D. Bazzacco,⁴ B. Birkenbach,¹ A. Bracco,⁵ B. Bruyneeel,⁶ L. Corradi,⁷ F. C. L. Crespi,⁵ G. de Angelis,⁷ M. Droste,¹ J. Eberth,¹ E. Farnea,^{4, b} E. Fioretto,⁷ C. Fransen,¹ A. Gadea,⁸ A. Giaz,⁵ A. Görgen,^{9, 10, 11} A. Gottardo,⁷ K. Hadyńska-Kleń,⁷ H. Hess,¹ R. Hetzenegger,¹ R. Hirsch,¹ P. R. John,¹² J. Jolie,¹ A. Jungclaus,¹³ W. Korten,¹⁰ S. Leoni,⁵ L. Lewandowski,¹ S. Lunardi,^{14, 4} R. Menegazzo,⁴ D. Mengoni,^{14, 4} C. Michelagnoli,¹⁵ T. Mijatović,¹⁶ G. Montagnoli,^{14, 4} D. Montanari,¹⁷ D. Napoli,⁷ Zs. Podolyák,¹⁸ G. Pollarolo,¹⁹ F. Recchia,^{14, 4} D. Rosiak,¹ N. Saed-Samii,¹ E. Şahin,²⁰ M. Siciliano,^{14, 7} F. Scarlassara,^{14, 4} M. Seidlitz,¹ P.-A. Söderström,²¹ A. M. Stefanini,⁷ O. Stezowski,²² S. Szilner,¹⁶ B. Szpak,²³ C. Ur,⁴ J. J. Valiente-Dobón,⁷ M. Weinert,¹ K. Wolf,¹ and K. O. Zell¹

¹*Institut für Kernphysik, Universität zu Köln, D-50937 Köln, Germany*

²*Istituto Nazionale di Fisica Nucleare, Sezione di Napoli, I-80126 Napoli, Italy*

³*Dipartimento di Matematica e Fisica, Università degli Studi della Campania “Luigi Vanvitelli”, viale A. Lincoln 5, I-8110 Caserta, Italy*

⁴*Istituto Nazionale di Fisica Nucleare, Sezione di Padova, I-35131 Padova, Italy*

⁵*Dipartimento di Fisica, Università di Milano and INFN Sezione di Milano, I-20133 Milano, Italy*

⁶*CEA Saclay, Service de Physique Nucleaire, F-91191 Gif-sur-Yvette, France*

⁷*Istituto Nazionale di Fisica Nucleare, Laboratori Nazionali di Legnaro, I-35020 Legnaro, Italy*

⁸*Instituto de Física Corpuscular, CSIC-Universidad de Valencia, E-46071 Valencia, Spain*

⁹*Department of Physics, University of Oslo, P. O. Box 1048 Blindern, N-0316 Oslo, Norway*

¹⁰*Institut de Recherche sur les lois Fondamentales de l’Univers – IRFU,*

CEA/DSM, Centre CEA de Saclay, F-91191 Gif-sur-Yvette Cedex, France

¹¹*Lawrence Berkeley National Laboratory, Berkeley, California 94720, USA*

¹²*Institut für Kernphysik, Technische Universität Darmstadt, D-64289 Darmstadt, Germany*

¹³*Instituto de Estructura de la Materia, CSIC, Madrid, E-28006 Madrid, Spain*

¹⁴*Dipartimento di Fisica e Astronomia, Università di Padova, I-35131 Padova, Italy*

¹⁵*Institut Laue-Langevin (ILL), 38042 Grenoble Cedex 9, France.*

¹⁶*Ruder Bošković Institute, HR-10 002 Zagreb, Croatia*

¹⁷*USIAS - Université de Strasbourg, IPHC-CNRS, F-67037 Strasbourg Cedex 2, France.*

¹⁸*Department of Physics, University of Surrey, Guildford, Surrey GU2 7XH, United Kingdom*

¹⁹*Dipartimento di Fisica Teorica dell’Università di Torino and INFN, I-10125 Torino, Italy*

²⁰*Department of Physics, University of Oslo, P. O. Box 1048 Blindern, N-0316 Oslo, Norway.*

²¹*Extreme Light Infrastructure-Nuclear Physics (ELI-NP), 077125 Bucharest-Magurele, Romania*

²²*Université de Lyon, Université Lyon-1, CNRS/IN2P3,*

UMR5822, IPNL, F-69622 Villeurbanne Cedex, France

²³*Henryk Niewodniczański Institute of Nuclear Physics PAN, PL-31342 Kraków, Poland*

(Dated: December 11, 2018)

The high-spin structures of ^{136}Ba and ^{137}Ba are investigated after multinucleon-transfer (MNT) and fusion-evaporation reactions. ^{136}Ba is populated in a $^{136}\text{Xe} + ^{238}\text{U}$ MNT reaction employing the high-resolution Advanced Gamma Tracking Array (AGATA) coupled to the magnetic spectrometer PRISMA at the Laboratori Nazionali di Legnaro, Italy, and in two $^9\text{Be} + ^{130}\text{Te}$ fusion-evaporation reactions using the High-efficiency Observatory for γ -Ray Unique Spectroscopy (HORUS) at the FN tandem accelerator of the University of Cologne, Germany. Furthermore, both isotopes are populated in an elusive reaction channel in the $^{11}\text{B} + ^{130}\text{Te}$ fusion-evaporation reaction utilizing the HORUS γ -ray array. The level scheme above the $J^\pi = 10^+$ isomer in ^{136}Ba is revised and extended up to an excitation energy of approx. 5.5 MeV. From the results of angular-correlation measurements, the $E_x = 3707$ - and $E_x = 4920$ -keV states are identified as the bandheads of positive- and negative-parity cascades. While the high-spin regimes of both ^{132}Te and ^{134}Xe are characterized by high-energy $12^+ \rightarrow 10^+$ transitions, the ^{136}Ba $E2$ ground-state band is interrupted by negative-parity states only a few hundred keV above the $J^\pi = 10^+$ isomer. Furthermore, spins are established for several hitherto unassigned high-spin states in ^{137}Ba . The new results close a gap along the high-spin structure of $N < 82$ Ba isotopes. Experimental results are compared to large-scale shell-model calculations employing the GCN50:82, Realistic SM, PQM130 and SN100PN interactions. The calculations suggest that the bandheads of the positive-parity bands in both isotopes are predominantly of proton character.

PACS numbers: 23.20.Lv, 27.60.+j, 29.40.Gx, 21.60.Cs

^a Corresponding author: levent.kaya@ikp.uni-koeln.de

^b Deceased.

I. INTRODUCTION

The $50 \leq Z, N \leq 82$ nuclei outside the doubly-magic nucleus ^{132}Sn are described within the valence space made up by the orbitals $0g_{7/2}$, $1d_{5/2}$, $1d_{3/2}$, $2s_{1/2}$, and $0h_{11/2}$. $A \approx 135$ nuclei near the $N = 82$ shell closure have the Fermi surface in the middle of the proton $d_{5/2}$ - $g_{7/2}$ subshell between $Z = 50$ and $Z = 64$ and offer a fertile region to deepen the understanding of the single-particle structure in the framework of the nuclear shell model and to study the evolution of different multi-quasiparticle configurations formed by a combined contribution of neutron holes and proton particles.

This work focuses on the high-spin structures of ^{136}Ba and ^{137}Ba with one and two valence neutron holes outside the $N = 82$ closed shell. Isomeric yrast $J^\pi = 10^+$ states accumulate in moderately neutron-rich Xe and Ba isotopes, as well as throughout the $N = 78$, $N = 80$, and $N = 82$ isotones above the $Z = 50$ shell closure. Along the $N = 80$ isotones, between ^{130}Sn and ^{142}Sm , these isomers are predominantly of $\nu h_{11/2}^{-2}$ character and seniority $v = 2$ [1–6]. The single-particle excitation energy of the $\nu h_{11/2}$ neutron orbital is observed to increase with proton number. This increase in single-particle energy is responsible for an increase of more than 1 MeV in the excitation energy of the yrast $J^\pi = 10^+$ state between ^{130}Sn and ^{140}Nd . From the proton $Z = 64$ subshell closure at ^{144}Gd onwards, $J^\pi = 10^+$ isomers are proposed to have two-proton $\pi h_{11/2}^2$ configurations [6, 7]. A compilation of high-spin level schemes above the isomeric $J^\pi = 10^+$ states along $N = 80$ is presented in Fig. 1(a).

The $10^+ \rightarrow 8^+$ isomeric transitions of ^{132}Te and ^{134}Xe have low energies of 22 and 28 keV, respectively [2]. High-spin states in the $N = 80$ isotone ^{132}Te were investigated up to spin $J^\pi = (17^+)$ with an excitation energy of 6.17 MeV [8]. The states along the $(16^+) \rightarrow (15^+) \rightarrow (14^+) \rightarrow (12^+) \rightarrow (10^+)$ cascade above the $J^\pi = 10^+$ isomer are predominantly of $\nu h_{11/2}^{-2}$ character. In ^{134}Xe , the high-spin structure above the isomeric $J^\pi = 10^+$ is known up to spin $J^\pi = (16^+)$ at 5.83 MeV. The high-spin yrast sequence is similar to ^{132}Te , despite an additional tentatively assigned $J^\pi = 13^+$ state between the $J^\pi = 12^+$ and 14^+ levels [9]. States of higher spins built on the $J^\pi = 10^+$ isomers involve the rearrangement of the valence protons since the configuration of the neutrons is already constrained. Therefore, both ^{132}Te and ^{134}Xe are characterized by high-energy $12^+ \rightarrow 10^+$ transitions of 900 and 1323 keV, respectively.

Pioneering work on ^{136}Ba focused on low-spin states up to the $J^\pi = 8^+$ state at $E_x = 2994$ keV, investigated via Coulomb excitation [10], β -decay [11], (n, γ) reactions [12], and ^9Be -induced fusion-evaporation reactions [13]. The $J^\pi = 10^+$ state at $E_x = 3357$ keV with a $\nu h_{11/2}^{-2}$ configuration was simultaneously discovered by Shizuma *et al.* [14] employing a $^{82}\text{Se} + ^{139}\text{La}$ deep-inelastic reaction at 450 MeV and by Valiente-Dobón *et al.* [3]

who populated ^{136}Ba in a $^{136}\text{Xe} + ^{198}\text{Pt}$ multinucleon-transfer reaction at a beam energy of 850 MeV. The groups reported half-lives of $T_{1/2} = 94(10)$ ns [14] and $T_{1/2} = 91(2)$ ns [3]. Valiente-Dobón *et al.* employed prompt-delayed correlations to identify seven γ -ray transitions feeding the $J^\pi = 10^+$ state and established a tentative high-spin structure. Contrary to ^{132}Te and ^{134}Xe , the next excited state is located only 349 keV above the 3357-keV isomeric state. According to shell-model calculations and systematics, it was assumed that the excitation pattern above the $J^\pi = 10^+$ state does not correspond to an $E2$ yrast sequence. Instead, a $J^\pi = 10^-, 11^-$ or 12^- assignment was suggested for the $E_x = 3707$ -keV state. However, angular-correlation measurements were not in the scope of the experiment [3].

Approaching the proton subshell closure, elaborate high-spin information from heavy-ion fusion-evaporation reactions are available for both ^{138}Ce and ^{140}Nd [15, 16]. Measurements of the $J^\pi = 10_1^+$ isomer's g -factors in both nuclei corroborated $\nu h_{11/2}^{-2}$ neutron-hole configurations [17]. In ^{138}Ce the $E2$ yrast sequence is interrupted by an intermediate $J^\pi = 11^+$ state, connecting $J = 12$ states of positive and negative parity with the 82(2)-ns $J^\pi = 10^+$ isomer. Going to higher spins, the level structure is significantly fragmented into several band structures dominated by different quasiparticle configurations [15].

The high-spin regime of ^{140}Nd is even more fragmented and explained by different two-neutron and two-proton excitations [16, 18, 19]. The 33(2)-ns $J^\pi = 10_1^+$ isomer decays via negative-parity states to the 0.6-ms $J^\pi = 7_1^-$ state. It is directly fed by $J^\pi = 11^-$ and $J^\pi = 10^-$ states [19]. A second $J^\pi = 10^+$ state was identified at 4155 keV, fed by positive-parity states [16]. Furthermore, ^{140}Nd exhibits a six-quasiparticle $J^\pi = 20^+$ isomer with a half-life of $T_{1/2} = 1.23(7)$ μs at 7430 keV [20].

Similar to the $J^\pi = 10^+$ isomers along $N = 80$, $J^\pi = 19/2^-$ isomers are a common feature of nuclei along $N = 81$ [4, 22, 23]. A compilation of several partial level schemes above the $J^\pi = 19/2^-$ isomers is shown in Fig. 1(b).

The level scheme of ^{133}Te is known up to 6.2 MeV with tentative spin assignments up to $J^\pi = (31/2^-)$ [25, 26]. A $J^\pi = (19/2^-)$ state at 1.610 MeV is found to be isomeric with an adopted half-life of $T_{1/2} = 100(5)$ ns [27]. In ^{135}Xe the high-spin regime is investigated up to 4.07 MeV, however, no spin and parities are known beyond the $J^\pi = 19/2^-$ state which is identified as an isomer with a half-life of $T_{1/2} = 9.0(9)$ ns [22].

Pioneering studies of ^{137}Ba mainly focused on low- and medium-spin states. Data were obtained utilizing β decay [28, 29], neutron-induced reactions [30], and Coulomb excitation [31]. The spins, parities and half-lives of the ground state and the $J^\pi = 11/2^-$ isomer at 661.659(3) keV with a half-life of 2.552(1) min are well established. First results on medium-spin states of ^{137}Ba were obtained by Kerek *et al.* in 1973 [32], via an α -induced reaction on a ^{136}Xe -enriched gas tar-

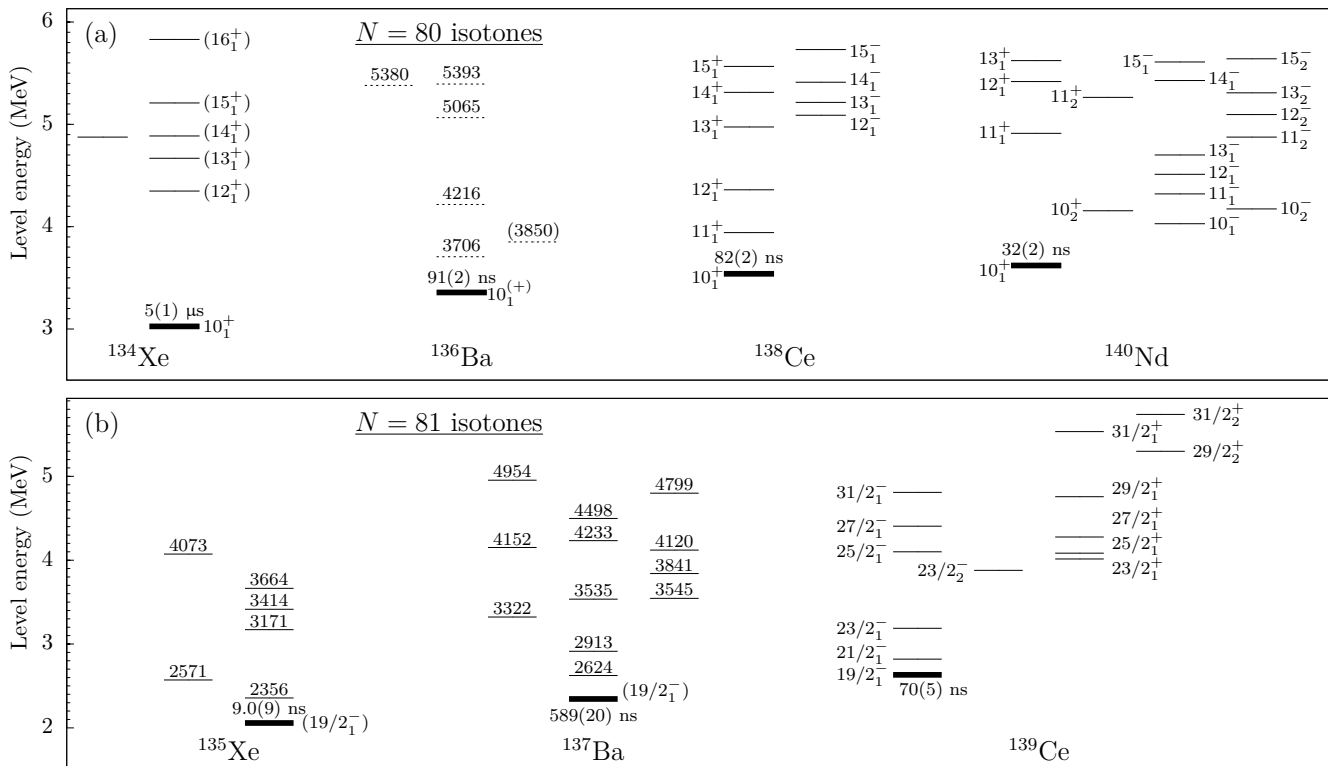


Figure 1. Comparison of high-spin states above (a) the $J^\pi = 10_1^+$ isomers along $N = 80$ and (b) above the $J^\pi = 19/2_1^-$ isomers along $N = 81$. There is a significant lack of information on spin assignments in ^{136}Ba and ^{137}Ba . Data taken from Refs. [3, 9, 15, 16, 19, 21–24].

152 get. An isomeric state at $E_x = 2350$ keV with possi- 179
 153 ble spin assignments $J^\pi = (15/2, 17/2, 19/2)$ and a half- 180
 154 life of $T_{1/2} = 590(100)$ ns was observed. This state 181
 155 was found to decay via a 120-1568-keV γ -ray cascade, 182
 156 finally populating the long-lived $J^\pi = 11/2_1^-$ isomer. 183
 157 The authors of the present work studied ^{137}Ba as a 184
 158 multinucleon-transfer and fusion-evaporation product using 185
 159 the Advanced Gamma-ray Tracking Array (AGATA) 186
 160 + PRISMA setup at LNL Legnaro, the GAMMAS- 187
 161 PHERE array at Lawrence Berkeley National Laboratory 188
 162 and the HORUS array at Cologne [22]. The level scheme 189
 163 was extended up to approx. 5 MeV excitation energy. 190
 164 Spin and parity assignments of high-spin states were not 191
 165 subject of the work [22]. 192

166 In ^{139}Ce the yrast negative-parity band based on the 193
 167 $J^\pi = 19/2^-$ isomer is well established up to an excita- 194
 168 tion energy of approx. 8 MeV [33, 34]. A band on top 195
 169 of a $J^\pi = 19/2^-$ isomer was initially proposed to be of 196
 170 negative parity [33, 34]. Recently, this structure was re- 197
 171 visited to be a positive-parity cascade built on top of a 198
 172 $J^\pi = 23/2^+$ bandhead decaying into the $J^\pi = 19/2^-$ 199
 173 isomer [24]. 200

174 Adding two more protons, a plethora of high-spin 201
 175 bands were discovered in ^{141}Nd [35, 36]. In an ear- 202
 176 lier experiment [4], delayed time distributions indicated 203
 177 a possible $J = 19/2^-$ isomeric state with $T_{1/2} = 26(5)$ ns 204
 178 at an energy of $2886 + x$ keV. However, this isomer was 205

not confirmed by subsequent studies [35, 36]. Moreover, 180
 no evidence of a positive-parity band connected to the 181
 $J^\pi = 19/2^-$ isomer was found to date. Thus, the typi- 182
 cal features of $J^\pi = 19/2^-$ isomers and the associated 183
 feeding high-spin structures along $N = 81$ could be first 184
 discontinued in ^{141}Nd .

185 Along the $N = 80$ and $N = 81$ isotones, spin and 186
 187 parity assignments are missing inter alia for ^{136}Ba and 188
 ^{137}Ba . Available information is limited to in part ten- 189
 tative excitation energies. Aim of the present work was 190
 to complement these earlier studies with spin and par- 191
 ity assignments of the high-spin states. The systemat- 192
 ics along the $N = 80$ chain suggest that the yrast $E2$ 193
 $12^+ \rightarrow 10^+$ cascades are first interrupted in ^{136}Ba accom- 194
 panied by a change in nuclear structure. This motivates 195
 a refined investigation of the high-spin features above the 196
 isomeric $J^\pi = 10^+$ state in ^{136}Ba and above the isomeric 197
 $J^\pi = 19/2^-$ state in ^{137}Ba .

197 In this Paper new results on ^{136}Ba and ^{137}Ba are 198
 199 presented. ^{136}Ba was populated in a $^{136}\text{Xe} + ^{238}\text{U}$ 200
 multinucleon-transfer (MNT) experiment employing the 201
 AGATA γ -ray spectrometer [37] in combination with the 202
 magnetic mass spectrometer PRISMA [38–40]. More- 203
 over, ^{136}Ba is investigated in two $^9\text{Be} + ^{130}\text{Te}$ and one 204
 $^{11}\text{B} + ^{130}\text{Te}$ fusion-evaporation experiment employing 205
 two different configurations of the High-efficiency Ob-
 servatory for γ -Ray Unique Spectroscopy (HORUS) [41]

at the Institute of Nuclear Physics, University of Cologne. ^{137}Ba was populated in the $^{11}\text{B} + ^{130}\text{Te}$ fusion-evaporation experiment. The HORUS experiments provide detailed information on $\gamma\gamma$ coincidences and angular correlations.

This paper is organized as follows: the experimental setup and data analysis of the experiments are described in Sec. II, followed by the experimental results in Sec. III. A comparison with large-scale shell-model calculations is presented in Sec. IV before the paper is completed with a summary and conclusions.

II. EXPERIMENTAL PROCEDURE

A. $^{136}\text{Xe} + ^{238}\text{U}$ multinucleon transfer

In this experiment, ^{136}Ba was populated in a $^{136}\text{Xe} + ^{238}\text{U}$ multinucleon-transfer experiment at the Laboratori Nazionali di Legnaro, Italy. The 6.84 MeV/nucleon ^{136}Xe beam, accelerated by the PIAVE+ALPI accelerator complex, impinged onto a 1 and a 2-mg/cm 2 ^{238}U target. An isotopic identification of the nuclei of interest was provided by the magnetic spectrometer PRISMA placed at the reaction's grazing angle of $\theta_{\text{lab}} = 50^\circ$. γ rays from excited states in both beam- and target like nuclei were detected with the AGATA γ -ray spectrometer [37] in the demonstrator configuration [42] placed 23.5 cm from the target position. The array consisted of 15 large-volume electronically segmented high-purity Ge (HPGe) detectors in five triple cryostats [43]. An event registered by the PRISMA focal-plane detector in coincidence with an AGATA event was taken as a trigger for the data acquisition. In this way the origin of the γ rays is distinguished, background from beta-decay is reduced and a major fraction of isomeric γ -ray transitions is suppressed.

Pulse-shape analysis of the digitized detector signals was applied to determine the individual interaction points within the HPGe shell [44], enabling the Orsay forward-tracking algorithm [45] to reconstruct the individual emitted γ -ray energies, determine the first interaction point of the γ ray in the germanium and, thus, the emission angle. Together with the kinematic information from PRISMA, a precise Doppler correction was performed. Further details on the analysis can be found in Ref. [46].

B. Part I: $^9\text{Be} + ^{130}\text{Te}$ fusion-evaporation reaction

In this experiment excited states in ^{136}Ba were populated in a $^9\text{Be} + ^{130}\text{Te}$ fusion-evaporation reaction. The FN Tandem accelerator of the Institute of Nuclear Physics, University of Cologne, provided a 40-MeV ^9Be beam. In this and two additional experiments, introduced in Sec. II B-II D, the target consisted of 99.3% enriched ^{130}Te with a thickness of 1.8 mg/cm 2 , evaporated onto a 120 mg/cm 2 thick Bi backing plus a 132 mg/cm 2

thick Cu layer for heat dissipation. In the three experiments, all reaction products were stopped inside the Bi backing. γ rays from excited reaction products were measured with a γ -ray array equipped with 11 high-purity germanium (HPGe) detectors, placed in rings at 45° (6 detectors) and 143° (5 detectors) with respect to the beam axis. In total, 9×10^7 $\gamma\gamma$ -coincidence events were collected.

C. Part II: $^9\text{Be} + ^{130}\text{Te}$ fusion-evaporation reaction

Another $^9\text{Be} + ^{130}\text{Te}$ fusion-evaporation reaction was performed at 43 MeV beam energy. The HORUS array comprised 14 HPGe detectors, six of them equipped with BGO Compton-suppression shields. The detectors were positioned on the eight corners and six faces of a cube. To reduce background radiation from X rays, each detector was shielded by 2-mm-thick sheets of lead and copper. Note that the relative efficiency of the first experiment (Sec. II B) exceeds the relative efficiency of the second experiment by a factor of more than 16 at a γ -ray energy of 100 keV. However, the total $\gamma\gamma$ -statistic is more than one order of magnitude higher than in the first experiment.

D. $^{11}\text{B} + ^{130}\text{Te}$ fusion-evaporation reaction

In the third experiment, ^{136}Ba and ^{137}Ba were populated via a $^{11}\text{B} + ^{130}\text{Te}$ fusion-evaporation reaction. Several fusion-evaporation codes predict a relative cross-section of $< 1\%$ for the evaporation channels of interest. The HORUS array was arranged similarly to the second ^{136}Ba experiment (Sec. II C). However, no additional shielding in front of the detectors were mounted. In total, 1.5×10^{10} $\gamma\gamma$ -coincidence events were recorded. Additional information about the experimental setup and the results of the $\gamma\gamma$ analysis of this experiment can be found in Ref. [22].

In all three fusion-evaporation experiments, γ -ray events were processed triggerless and recorded utilizing the synchronized 80-MHz XIA $^{\text{TM}}$ Digital Gamma Finder (DGF) data-acquisition system. The data were analyzed offline using the codes SOCO-v2 [47] and TV [48].

The HORUS spectrometer arranged in the cube configuration allows to investigate multipole-mixing ratios of transitions between excited states with the $\gamma\gamma$ angular-correlation code CORLEONE [49, 50] based on the phase convention by Krane, Steffen, and Wheeler [51, 52]. Different hypotheses of involved spins J_1, J_2, J_3 and multipole-mixing ratios δ_1, δ_2 of two coincident γ rays in a cascade $J_1 \xrightarrow{\delta_1} J_2 \xrightarrow{\delta_2} J_3$ are evaluated by χ^2 fits of the correlation function $W(\Theta_1, \Theta_2, \Phi) = W(J_1, \delta_1, J_2, \delta_2, J_3)$ to experimental intensities in eight different correlation groups, each associated with detector pairs at angles $\Theta_{1,2}$ with respect to the beam axis and a relative angle Φ between the planes spanned by the detectors and the beam axis. Note that the correlation intensities also depend

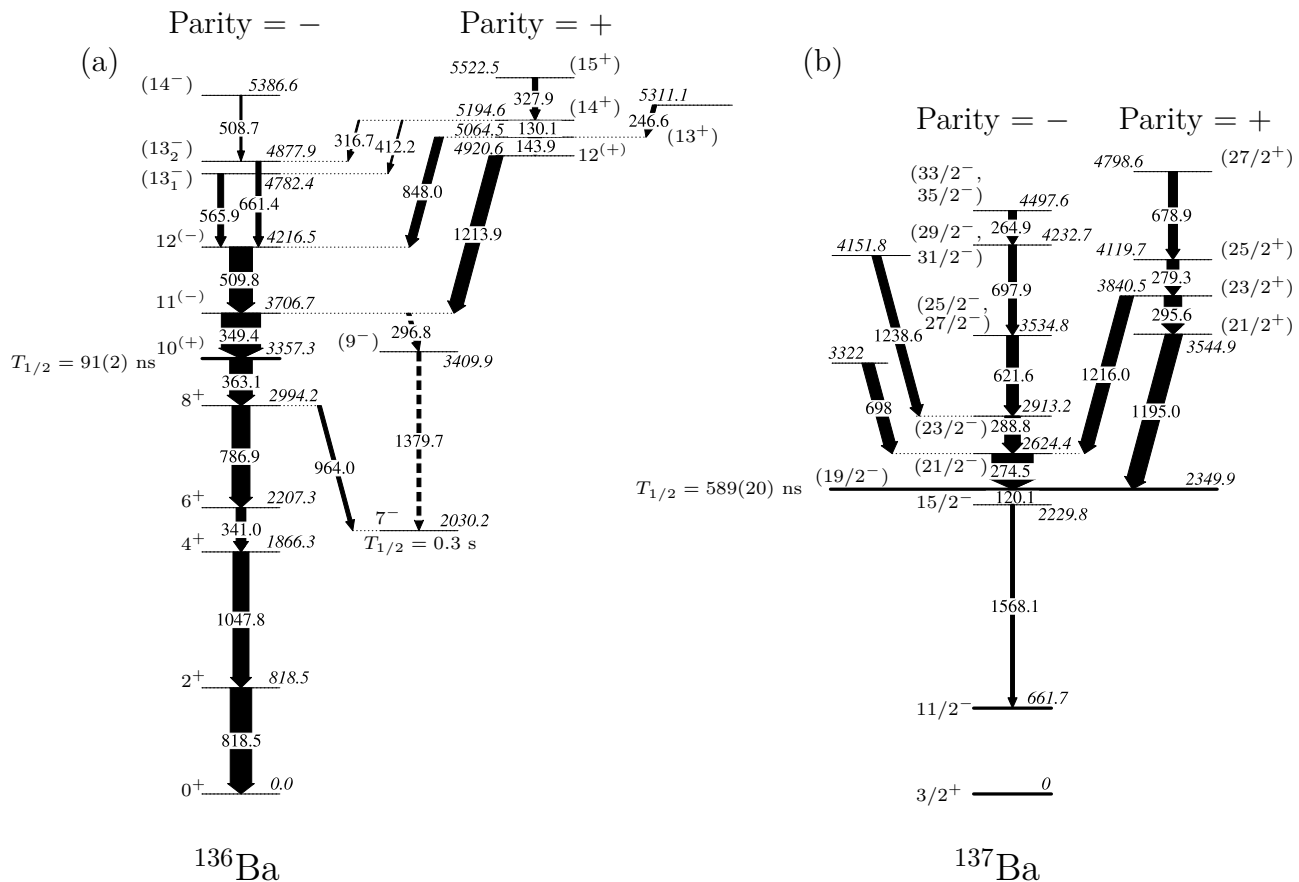


Figure 2. (a) Level scheme assigned to ^{136}Ba in the present work. Transitions and excitation energies are given in keV. γ -ray intensities above the $J^\pi = 10^+$ isomer are deduced from the $^9\text{Be} + ^{130}\text{Te}$ experiment and normalized to the 349-keV transition. (b) Level scheme assigned to ^{137}Ba and normalized to the 275-keV transition. Transitions and excitation energies are taken from the previous work, using the same $^{11}\text{B} + ^{130}\text{Te}$ experiment, presented in Ref. [22]. Tentative assignments are given in brackets and dashed lines. In both isotopes new spin/parity assignments are based on the spin/parity assignments of the isomeric 3357.3 keV state in ^{136}Ba given in Ref. [14] and on the spin/parity assignments of the isomeric 2349.9 keV state in ^{137}Ba given in Refs. [22, 23]. See text for details.

309 on the orientation parameter σ : the fusion-evaporation
 310 reaction orients the spin of the initial level J_1 with re-
 311 spect to the beam axis. The orientation is described by
 312 a Gaussian distribution of the magnetic substates with
 313 mean value $\langle m \rangle = 0$ and variance σ^2 . The width of
 314 the alignment distribution was found to be constant at
 315 $\sigma = 2.1$. More details on the angular-correlation analysis
 316 with CORLEONE are given in Refs. [53, 54]

III. EXPERIMENTAL RESULTS

A. ^{136}Ba

319 The level scheme of ^{136}Ba deduced in the four experi-
 320 ments is presented in Fig. 2(a). New parity assignments
 321 of states above the $J^\pi = 10^+$ isomer are based on the parity
 322 assignments of the isomeric 3357-keV state in ^{136}Ba
 323 given in Refs. [3, 14]. The $J^\pi = 10^+$ assignment with

324 the tentative positive parity is strongly supported by sys-
 325 tematics, shell-model calculations and measured DCO ra-
 326 tios [3, 14].

327 The Doppler-corrected AGATA singles γ -ray spectrum
 328 of ^{136}Ba in the $^{136}\text{Xe} + ^{238}\text{U}$ experiment is shown in
 329 Fig. 3(a). The mass spectrum along the Ba isotopes
 330 identified with PRISMA and the applied gate on ^{136}Ba
 331 is shown in the inset Fig. 3(b). Transitions at γ -ray ener-
 332 gies of 529, 602, and 807 keV are contaminants from the
 333 $+4n$ channel ^{140}Ba . Moderately weak lines at 262 and
 334 1399 keV can be associated to known transitions in the
 335 isobar ^{136}Cs . Due to the restriction to prompt events
 336 in the time-difference spectrum between PRISMA and
 337 AGATA, i.e. $\Delta t_{\text{PRISMA-AGATA}} \approx 16$ ns, transitions be-
 338 tween states below the $E_x = 3357$ keV $J^\pi = 10^+$ isomer
 339 are found to be suppressed in the spectrum. The largest
 340 peaks in the spectrum are located at 349 and 510 keV.
 341 In previous works both transitions were placed on top
 342 of the 3357-keV isomer to form a cascade deexciting the

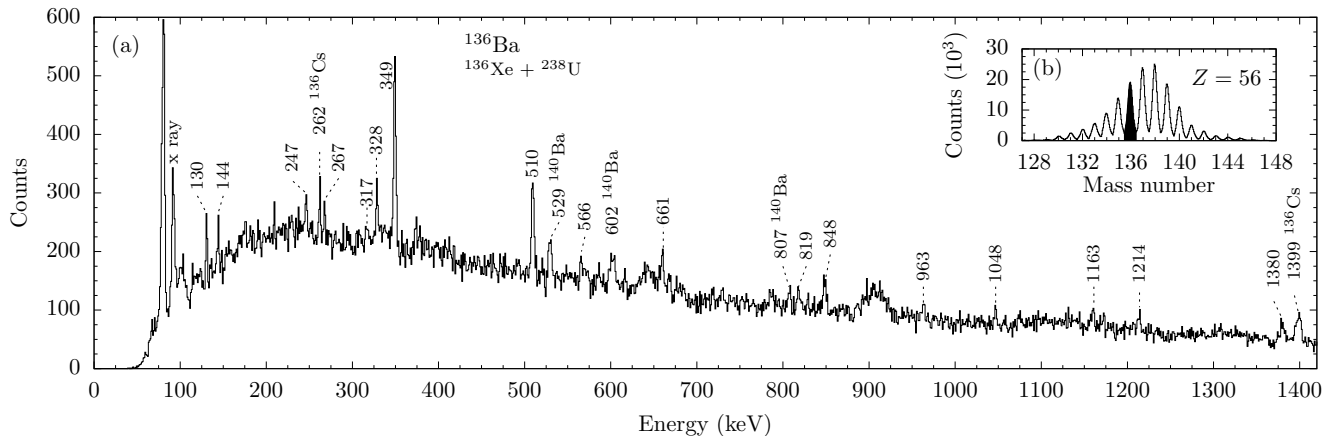


Figure 3. (a) Doppler-corrected γ -ray spectrum gated on ^{136}Ba identified in PRISMA in the $^{136}\text{Xe} + ^{238}\text{U}$ experiment. γ -ray energies are given in keV. (b) Mass spectrum of Ba isotopes identified with PRISMA. The applied mass gate on ^{136}Ba is marked black. A gate on the prompt time peak between AGATA and PRISMA is applied to reduce random background.

4217-keV state [3, 14]. Further peaks at 130, 144, 247, 328, 848, and 1214 keV are consistent with those found by Valiente-Dobón *et al.* [3]. However, the placement of 130- and 247-keV transitions was unknown in the level scheme of the previous work due to similar relative peak intensities.

Measured intensities of coincident γ rays from the HORUS experiments are summarized in the right-hand side of Tab. I. All intensities are efficiency-corrected and normalized to the intensity of the 349-keV transition. Intensities are extracted from the $^9\text{Be} + ^{130}\text{Te}$ experiment ($I_\gamma^{^9\text{Be}}$) as well as from the $^{11}\text{B} + ^{130}\text{Te}$ experiment ($I_\gamma^{^{11}\text{B}}$). The independently measured intensities show a consistent assignment of states and transitions. The uncertainties in the transition energies are ± 0.5 keV. Spin/parity assignments are supported by angular-correlation measurements and shell-model calculations. Various HORUS background-subtracted prompt $\gamma\gamma$ -coincidence spectra from the first $^9\text{Be} + ^{130}\text{Te}$ experiment (see Sec. II B) with gates on transitions above the $J^\pi = 10^+$ isomer are shown in Figs. 4(a)-(d). Contaminant transitions in the spectrum gated on the 328 keV transition (Fig. 4(c)) stem from $35/2^- \rightarrow 33/2^-$ transition in ^{135}Ba [55]. Coincident transitions deexciting the isomeric $E_x = 3357$ -keV state are suppressed in intensity, due to the prompt $\gamma\gamma$ -coincidence time gate of 175 ns.

Figure 4(a) presents the γ -ray spectrum with a gate on the 349-keV transition. Coincidences are labeled with filled arrow heads. The spectrum exhibits anticipated coincidences at 144, 328, 510, 848, and 1214 keV. Unassigned peaks at 130, 247, 566, and 661 keV, observed in the AGATA experiment, are coincident to the 349-keV transition. In the previous work [3], the 144 and 1214 keV γ -rays are arranged to form a state at $E_x = 3850$ keV. A gate on the 848-keV transition is shown in Fig. 4(b). The absence of the 144-1214-keV cascade requires the 848-keV transition to be placed parallel to this cascade.

The intensity of the 1214-keV peak in the $\gamma\gamma$ -coincidence spectrum gated on 349 keV exceeds the one of the 144-keV line. Moreover, the 144-1214-keV cascade corresponds to the sum energy of the 848-510-keV cascade. Therefore, in accordance with the measured intensity relations of the 1214- and 144-keV transitions, the 144-keV transition has to be placed on top of the 1214-keV transition, resulting in a new state at 4921 keV excitation energy.

Coincidences with the 848-keV and 1214-keV transitions as well as intensity balances require a placement of the 130, 247, and 328-keV transitions above the 5065-keV state. Since the 130-keV transition is mutually coincident with the 328-keV transition (cf. Fig 4(c)), both transitions form a 328-130 keV cascade on top of the $E_x = 5065$ -keV state. The ordering of the 328- and 130-keV transitions agrees with the intensity balance measured in the $\gamma\gamma$ projections gated on the 144-, 349-, 848-, and 1214-keV transitions. Additionally, Fig. 4(d) shows that the 247-keV transition is not coincident with the 328-130-keV cascade. Consequently, the 247-keV transition is placed parallel to the 328-130-keV cascade to establish a state at $E_x = 5311$ keV.

Moreover, Fig. 4(a) shows two additional coincidences at 566 and 661 keV, however, both transitions are neither coincident with the transitions at 848 and 328 keV, nor with the 247-keV transition (cf. Fig. 4(a)-(d)). Due to insufficient statistics we use the higher $\gamma\gamma$ statistics from the second $^9\text{Be} + ^{130}\text{Te}$ experiment (see Sec. II C) to place the 566- and 661-keV transitions in the level scheme. We remind the reader that although the total $\gamma\gamma$ statistics of this experiment is higher, the efficiency at small energies is limited due to the use of absorbers.

Figures 4(e)-(g) show double-gated $\gamma\gamma\gamma$ -coincidence and sums of double-gated $\gamma\gamma\gamma$ -coincidence spectra. Both the 566- and 661-keV transitions emerge in the $\gamma\gamma\gamma$ projection gated on 510 and 349 keV, as displayed in Fig. 4(e). Hence, the transitions have to feed the 4217-keV state. Since the 566- and 661-keV transitions are not

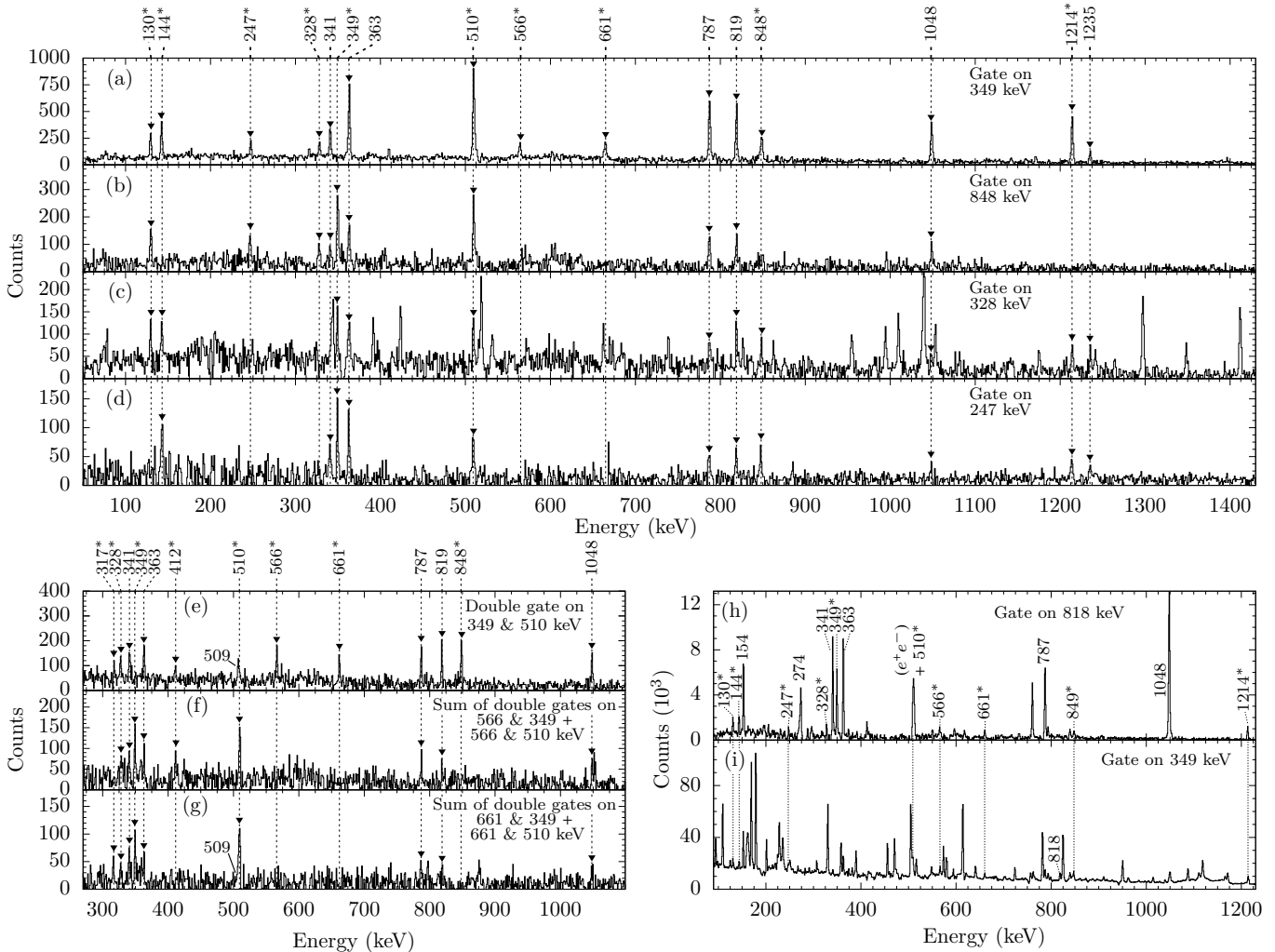


Figure 4. Prompt $\gamma\gamma$ double-coincidence spectra from the first ${}^9\text{Be} + {}^{130}\text{Te}$ experiment (see Sec. II B) with gates on (a) 349, (b) 848, (c) 328, and (d) 247 keV. Transitions above the $J^\pi = 10^+$ isomer are marked with asterisks. Coincidences are labeled by filled arrow heads. Contaminant transitions in the spectrum gated on the 328 keV stem from transitions in ${}^{135}\text{Ba}$. $\gamma\gamma$ triple-coincidence spectra from the second ${}^9\text{Be} + {}^{130}\text{Te}$ experiment (see Sec. II C) with (e) a double gate on 349 & 510 keV, a sum of double-gated triples coincidence spectra gated on (f) 566 & 510 and 566 & 349 keV, and a similar sum spectra gated on (g) 661 & 510 and 661 & 349 keV. Prompt $\gamma\gamma$ double-coincidence spectra with a gate on (h) 818 and (i) 349 keV from the ${}^{11}\text{B} + {}^{130}\text{Te}$ experiment (see Sec. II D). The gate on 349 keV is contaminated with transitions from ${}^{137}\text{La}$.

418 in mutual coincidence (cf. Fig. 4(f)-(g)) both have to be
419 placed parallel, directly feeding the $E_x = 4217$ -keV state.

420 Furthermore, the spectrum gated on the 510-349-keV
421 cascade (c.f. 4(e)) reveals weak lines at 317 and 412 keV.
422 The 317-keV transition corresponds to the energy difference
423 between the new established states at 4878 and
424 5195 keV, while the 412-keV transition corresponds to the
425 transition between the new established states at 4782
426 and 5195 keV. As expected, the 412-keV transition is
427 only observed in coincidence with the 566-keV transition
428 (c.f. 4(f)) and the 317-keV transition is in coincidence
429 with the 661-keV transition (c.f. 4(g)).

430 A further 509-keV transition is in coincidence with the
431 510-349-keV cascade, as shown in Fig. 4(e). The centroid
432 of this peak is clearly separated by 0.9 keV from the 510-

433 keV peak position in Fig. 4(f). Since the Full Width at
434 Half Maximum (FWHM) of the coincident 510-keV transi-
435 tion gated on 566-keV is broader than the similar peak
436 gated on 661-keV, the 509-keV transition is identified as
437 another transition above the 4878-keV state.

438 An intense 1380-keV transition is observed in the
439 AGATA spectrum in Fig. 3. In accordance with previ-
440 ous studies performed with the AGATA dataset [9, 22],
441 a transition from a contaminant can be excluded. In the
442 HORUS experiment this transition is observed to be co-
443 incidence with transitions stemming from the $5^- \rightarrow 2^+$
444 decay in ${}^{134}\text{Ba}$ and in coincidence with a 297-keV transi-
445 tion. Assuming a 1380-keV transition above the $J^\pi = 7^-$
446 isomer at $E_x = 2030$ keV, the energy difference between
447 the 3707-keV state and a proposed $E_x = 3410$ keV state

Table I. Energies, spin assignments and relative in-beam intensities for γ -ray transitions in ^{136}Ba above the $J^\pi = 10_1^+$ isomer at $E_x = 3357.3$ keV. Fitted energies and relative intensities normalized to the 349.4-keV transition are taken from two experiments: $I_\gamma^{^{11}\text{B}}$ from $^{11}\text{B} + ^{130}\text{Te}$ and $I_\gamma^{^9\text{Be}}$ from $^9\text{Be} + ^{130}\text{Te}$.

E_γ (keV)	E_i (keV)	E_f (keV)	I_i^π	I_f^π	$I_\gamma^{^{11}\text{B}}$	$I_\gamma^{^9\text{Be}}$
130.1	5194.6	5064.5	(14 ⁺)	(13 ⁺)	20(2)	18(2)
143.9	5064.5	4920.6	(13 ⁺)	12 ⁽⁺⁾	29(2)	23(2)
316.7	5194.6	4877.9	(14 ⁺)	(13 ₁ ⁻)	9(2)	weak
246.6	5311.1	5064.5	—	(13 ⁺)	12(3)	10(1)
327.9	5522.5	5194.6	(15 ⁺)	(14 ⁺)	12(3)	13(2)
349.4	3706.7	3357.3	11 ⁽⁻⁾	10 ⁽⁺⁾	$\equiv 100$	$\equiv 100$
412.2	5194.6	4782.4	(14 ⁺)	(13 ₁ ⁻)	10(2)	weak
508.7	5386.6	4877.9	(14 ⁻)	(13 ₂ ⁻)	weak	weak
509.8	4216.5	3706.7	12 ⁽⁻⁾	11 ⁽⁻⁾	62(9)	63(7)
565.9	4782.4	4216.5	(13 ₁ ⁻)	12 ⁽⁻⁾	25(3)	15(1)
661.4	4877.9	4216.5	(13 ₁ ⁻)	12 ⁽⁻⁾	20(2)	13(1)
848.0	5064.5	4216.5	(13 ⁺)	12 ⁽⁻⁾	30(3)	27(3)
1213.9	4920.6	5064.5	12 ⁽⁺⁾	11 ⁽⁻⁾	42(4)	35(3)

corresponds to 297 keV. Accordingly, the 297-1380-keV cascade is tentatively placed above the $J^\pi = 7^-$ isomer, connecting the $E_x = 3707$ -keV state with the isomer. This assignment is further supported by the recent observation of a similar 415-1099-keV cascade on top of the $J^\pi = 7^-$ isomer in the isotone ^{134}Xe [9].

^{136}Ba was also populated in the $^{11}\text{B} + ^{130}\text{Te}$ fusion-evaporation experiment with significantly lower relative cross section (see Sec. IID). Figs. 4(h)-(i) show exemplary prompt $\gamma\gamma$ -coincidence spectra with gates on the 818- and 349-keV transitions. Besides dominant coincident transitions originating from the 348-keV ($33/2^+ \rightarrow 31/2^-$) decay in ^{137}La [56], also transitions from ^{136}Ba , including the new established transitions, are observed well above the background. Intensities ($I_\gamma^{^{11}\text{B}}$), normalized to the intensity of the 349-keV transition, are listed in Tab. I. The observed coincidences in the $^{11}\text{B} + ^{130}\text{Te}$ experiment are consistent with the aforementioned results and strongly support the new results on ^{136}Ba .

The detectors in the HORUS setup of the $^9\text{Be} + ^{130}\text{Te}$ experiment (see Sec. IIC) were arranged in a cube configuration, yielding five rings at relative angles of 35° (ring 1), 45° (ring 2), 90° (ring 3), 135° (ring 4), and 145° (ring 5) with respect to the beam axis. Fig. 5(a) shows the distribution of the measured singles γ -ray intensity of the well-known 1052-keV transition ($19/2^- \xrightarrow{E2} 15/2^-$) in ^{135}Ba in the different rings, normalized to the intensity of ring 3. Moreover, Fig. 5(b) shows a similar distribution for the 391-keV transition ($21/2^- \xrightarrow{E1} 19/2^-$) in ^{135}Ba . Both distributions are compared with theoretical pure dipole- and quadrupole- transition hypotheses as described by Yamazaki *et al.* [57]. Both angular distri-

butions are symmetric around 90°. The intensity of the quadrupole 1052-keV transition ($\Delta I = 2$) in Fig. 5(a) is maximum along the beam axis, whereas the one of the dipole 391-keV transition ($\Delta I = 1$) in Fig. 5(b) is maximum perpendicular to the beam axis, demonstrating spin alignment with respect to the beam axis.

The characteristic investigation of dipole and quadrupole radiation signatures in the HORUS experiment is used to determine the multipolarity of the 349-keV transition in ^{136}Ba . In Fig. 5(c) the singles γ -ray intensity distribution of the 349-keV transition is compared to different theoretical pure dipole and quadrupole distributions for spins $J = 10, 11, 12$ of the $E_x = 3707$ -keV state. The $12 \xrightarrow{\Delta I=2} 10$ and $10 \xrightarrow{\Delta I=1} 10$ hypotheses can be clearly rejected. Since the 349-keV γ ray has a Weisskopf half-life estimate of $T_{1/2} = 0.17$ ms for an $E3$ transition, an $E3$ character is disregarded. Possible, $10 \xrightarrow{\Delta I=2} 10$ and $11 \xrightarrow{\Delta I=2} 10$ hypotheses show large discrepancies between theoretical and experimental values. Moreover, a mixed dipole-quadrupole transition with initial spin of $J^\pi = 10^+$ does not provide a better agreement. Hence, the four abovementioned hypotheses can be rejected. A pure dipole decay and an initial spin of $J = 11$ for the $E_x = 3707$ -keV state yields the best agreement with the experimental intensity distribution.

Based on the assigned spin of the $E_x = 3707$ -keV state, further spin hypotheses are tested for the $E_x = 4217$ -keV and the newly established $E_x = 4921$ -keV states applying the procedure of $\gamma\gamma$ angular correlation measurements discussed in Sec. II. Angular-distribution functions $W(\Theta_1, \Theta_2, \Phi)$ of two coincident γ -ray transitions are fitted to experimental γ -ray intensity distributions obtained by gates on depopulating transitions in the $\gamma\gamma$ -coincidence matrices of eight angular-correlation groups. Figure 5(d) shows a benchmark angular-correlation fit of the 727-keV decay, gated on the 773-keV $E2$ transition in ^{132}Xe . The fit of a $5^+ \xrightarrow{\delta} 4^+ \xrightarrow{E2} 2^+$ hypothesis yields a good agreement with the experimental distribution. Moreover, the obtained $E2/M1$ multipole-mixing ratio of $\delta_{\text{exp.}} = 0.44(7)$ agrees well with the evaluated value of $\delta = 0.41_{-8}^{+7}$ [58].

Similarly, keeping the spin of the 3357- and the 3707-keV state in ^{136}Ba fixed, spins of $J = 11, 12$, and 13 were tested for the $E_x = 4217$ -keV state. One multipole-mixing ratio δ in the $J_1 \xrightarrow{\delta_1} J_2 \xrightarrow{\delta_2} J_3$ cascade is fixed while the other is varied in order to avoid an overdetermination of the fit. For a parity-changing $E1$ transition, a multipole-mixing ratio in the order of $\delta \approx 0$ is expected. Scenarios of $11 \xrightarrow{\delta_1=0} 11 \xrightarrow{\delta_2} 10$ and $12 \xrightarrow{\delta_1=0} 11 \xrightarrow{\delta_2} 10$ for the 510-349-keV cascade yield χ^2 values of 10 and 14. Obviously, a parity-changing 510-keV $E1$ transition can be rejected. Moreover, a $13 \xrightarrow{\delta_1=0} 11 \xrightarrow{\delta_2} 10$ assumption does not fit the experimental data, which excludes an $E2$ transition with 510 keV. Vice versa, keeping $\delta_2 = 0$ fixed, a much better agreement is obtained. Fig. 5(e) visualizes the angular-correlation distribution

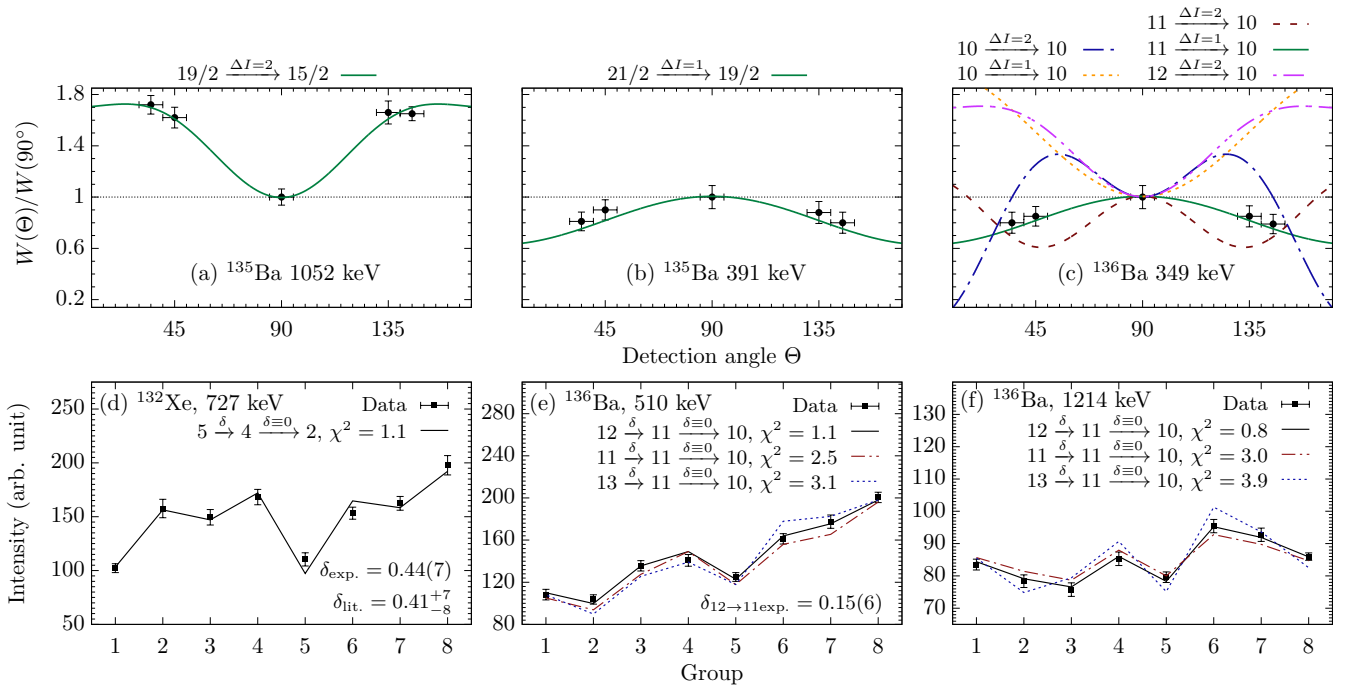


Figure 5. (Color online) Benchmark angular distribution of (a) the 1052-keV ($19/2^- \rightarrow 15/2^-$) γ -ray transition and (b) the 391-keV ($21/2^- \rightarrow 19/2^-$) γ -ray transition, both in ^{135}Ba . Experimental values (data points) are compared to pure dipole and quadrupole hypotheses (solid lines). (c) Angular distribution of the 349-keV transition, feeding the $J^\pi = 10^+$ isomer in ^{136}Ba . Several pure dipole and quadrupole hypotheses (lines) are plotted. (d) Benchmark $\gamma\gamma$ angular-correlations for the $5_1^+ \rightarrow 4_1^+ \rightarrow 2_1^+$ (727-773-keV) cascade in ^{132}Xe . Experimental values (data points) are compared to calculated angular-correlation functions $W(\Theta_1, \Theta_2, \Phi)$ (lines) for eight correlation groups using the code CORLEONE. Investigation for (e) the 510-349-keV cascade and (f) the 1214-349-keV cascade in ^{136}Ba . Several spin hypotheses are plotted.

536 for the 510-349 keV cascade in ^{136}Ba with respect to the
 537 different groups. The $12 \xrightarrow{\delta_1} 11 \xrightarrow{\delta_2=0} 10$ hypothesis with
 538 $\delta_1 = -0.15(6)$ ($\chi^2 = 1.1$) gives the best agreement with
 539 the experimental $W(\Theta_1, \Theta_2, \Phi)$ distribution in all correlation
 540 groups. Thus, a spin of $J = 12$ is assigned to the
 541 4217-keV state. Apart from that, similar fits assuming a
 542 larger fixed δ_2 value for the 349-keV transition yield significantly
 543 worse χ^2 values of the $12 \xrightarrow{\delta_1} 11 \xrightarrow{\delta_2} 10$ hypothesis
 544 (i.e. $\delta_2 \equiv \pm 0.05$; $\chi^2 > 2.6$ and $\delta_2 \equiv \pm 0.1$; $\chi^2 > 3.3$).
 545 Hence, on the basis of a pure-dipole character for the 349-
 546 keV γ -ray as shown in Fig. 5(c) and the overall agreement
 547 with the shell-model calculations presented in Sec. IV A,
 548 a parity changing $E1$ transition is proposed leading to a
 549 negative parity assignment of the 3707-keV state.

550 Employing the same method, the spin of the newly estab-
 551 lished excited state at $E_x = 4921$ keV is determined,
 552 as shown in Fig. 5(f). Spins of $J = 11$, 12, and 13 are
 553 tested. Assuming $\delta_2 = 0$, the 1214-349-keV cascade is
 554 best reproduced by a $12 \xrightarrow{\delta_1} 11 \xrightarrow{\delta_2} 10$ sequence with
 555 $\delta_1 = -0.01(12)$. Vice versa, keeping $\delta_1 = 0$ fixed, δ_2 is
 556 determined to be in agreement with zero. The obtained
 557 χ^2 values of both fits are similar, showing the mutual
 558 consistency of both hypotheses. Consequently, similar to
 559 the negative-parity $E_x = 4217$ -keV state, the $E_x = 4920$ -
 560 keV state has a spin of $J = 12$. The pure dipole charac-
 561 ter of the 1214-keV transition suggests a $E1$ character of

562 this transition, indicating that the $E_x = 4920$ -keV state
 563 has different spin than the $E_x = 3707$ -keV state and is
 564 therefore most probably of positive parity. Moreover, the
 565 independently measured 1214-349-keV cascade supports
 566 a pure-dipole $E1$ 349-keV transition.

567 The $\gamma\gamma$ angular-correlation analysis is further exploited
 568 to verify the validity of the 297-1380-keV cascade on top
 569 of the $J^\pi = 7^-$ isomer. The spin of the initial $J = 11$
 570 state and that of the final $J = 7$ state are fixed. A spin
 571 assumption of $J = 9$ for the $E_x = 3410$ -keV state yields
 572 a χ^2 value of 1.8, compared to χ^2 values of 2.2 and 2.3
 573 for $J = 10$ and $J = 8$ hypotheses. Since an $E3$ or $M2$
 574 transition in this cascade would corroborate another iso-
 575 mer, a spin assignment of $J = 9$ for the $E_x = 3410$ -keV
 576 state is necessary to keep a prompt decay character. Con-
 577 sequently, the angular-correlation measurement supports
 578 the 297-1380-keV cascade in ^{136}Ba .

579 B. ^{137}Ba

580 In a previous work by this group [22], the level scheme
 581 of ^{137}Ba above the $J^\pi = 19/2^-$ isomer was extended to
 582 the structure presented in Fig. 2(b), using the $\gamma\gamma$ coin-
 583 cidences from the $^{11}\text{B} + ^{130}\text{Te}$ experiment introduced in
 584 Sec. II D. This paper focuses on the angular-distribution

and angular-correlation analysis of this data set. Note that the new determined spins and parity of the high-spin states is based on the tentative $J^\pi = 19/2^-$ assignment of the isomeric 2350 keV state in ^{137}Ba given in Refs. [22, 23]. However, the assignment is strongly supported by systematics and shell-model calculations.

Due to the low cross section of the $p3n$ evaporation channel, the basis of the data analysis are double- γ HPGe coincidences to reduce the complexity of the γ -ray spectra of the different rings of the HORUS setup. The fusion-evaporation reaction orients the spin of the initial level with respect to the beam axis. However, according to the very long half-life of the $J^\pi = 19/2^-$ state, the 120-1568-keV cascade is no longer aligned with respect to the beam axis; it decays instead isotropic. Thus, a γ -ray gate on 1568 keV does affect the alignment with respect to the beam axis for coincident transitions above the isomer.

To verify that the spins above the isomer are still aligned with respect to the beam axis, a benchmark angular γ -ray distribution of the well-known 1172-keV ($23/2^- \xrightarrow{E2} 19/2^-$ [56]) transition in ^{137}La is shown in Fig. 6(a). The intensities in the different rings are extracted from the corresponding γ -ray spectra, gated on the 782-keV ($15/2^- \rightarrow 11/2^-$) transition, located below the $J^\pi = 19/2^-$ ($T_{1/2} = 360(40)$ ns [59]) isomer. A good agreement between measured and theoretical intensity distribution of a pure quadrupole transition is demonstrated.

In ^{137}Ba the $J^\pi = 19/2^-$ ($T_{1/2} = 0.589(20)$ μs [22]) isomer decays via a 120-1568-keV cascade. Applying a 1568-keV gate to all rings, comparisons between measured and theoretical angular distributions for the 275- and 1195-keV transitions in ^{137}Ba are shown in Figs. 6(b) and 6(c). In both cases, the highest intensity was measured in the detectors perpendicular to the beam axis, what is opposite to the distribution of the benchmark quadrupole transition presented in Fig. 6(a). Therefore, both experimentally determined intensity distributions are incompatible with a quadrupole $23/2 \xrightarrow{\Delta I=2} 19/2$ transition. Also an $E3$ transition can be clearly rejected for both γ rays, since the Weisskopf half-life estimate is several orders of magnitude larger compared to a competitive quadrupole transition. Moreover, pure as well as mixed quadrupole/dipole $19/2 \xrightarrow{\Delta I=1,2} 19/2$ transitions do not fit the experimental data. Overall, a $J = 21/2$ hypothesis for both initial states match the experimental values best.

Spins of the 2913- and 3841-keV states are determined using the $\gamma\gamma$ -coincidence angular-correlation technique. The number of groups has to be reduced in order to perform angular-correlation measurements in the elusive Ba channels. To ensure the quality of the angular-correlation analysis, a benchmark fit of the well-established $4^+ \rightarrow 2^+ \rightarrow 0^+$ cascade in ^{136}Ba is presented in Fig. 6(d). The $E2$ character of the 1048-keV transition is well reproduced.

The singles γ -ray angular-distribution measurement suggested a spin of $J = 21/2$ for both the 2624- and 3545-keV state (c.f. Fig. 6(b)-(c)). Consequently, the spin values of the 2913- and 3841-keV states are limited to $J = 21/2, 23/2,$ and $25/2$. Fig. 6(e) shows the experimental angular-correlation distribution of the 289-keV transition in the different groups, gated on the 275-keV transition. Assuming a vanishing multipole-mixing ratio ($\delta_1 = 0$) of the 289-keV transition and a variable δ_2 value of the 275-keV transition, fits of the three aforementioned hypotheses results in χ^2 values larger than 4. Furthermore, fixing the 275-keV transition to a dipole character ($\delta_2 = 0$) and varying the δ_1 value of the 289-keV transition, χ^2 values larger than 6 were obtained. Since the 275- and 289-keV transitions are incompatible with a multipole-mixing ratio of zero, a parity-changing $E1$ character of the 275- or 289-keV transition can be ruled out. Likewise, a parity-conserving $E2$ character with a spin change from $J = 25/2$ to $J = 21/2$ for the 289-keV transition is not compatible with the experimental distribution. Fig. 6(e) shows two examples for fits with corresponding χ^2 values of 12.7 and 8.2. Since the 289-275-keV cascade built on the $J^\pi = 19/2^-$ state has no parity-changing character, we propose negative-parity states $J^\pi = 21/2^-$ at $E_x = 2624$ -keV and $J^\pi = 23/2^-$ at $E_x = 2913$ -keV.

Fig. 6(f) shows the experimentally deduced angular-correlation intensity distribution for the coincident γ rays at 1195 and 296 keV, compared to calculated values for different scenarios of the spin and parity of the 3841-keV state. Fixing the spin value of the 3545-keV state to $J = 21/2$, hypotheses with pure dipole character ($21/2 \xrightarrow{\delta_1=0} 21/2$ or $23/2 \xrightarrow{\delta_1=0} 21/2$) as well as a pure quadrupole character ($25/2 \xrightarrow{\delta_1=0} 21/2$) yield a limited agreement with the data. Instead, a good match is obtained by assuming a dominant dipole component ($\delta_2 = 0$) for the $21/2 \rightarrow 19/2$ 1195-keV transition and a non-zero δ_1 value for the 296-keV transition. A hypothesis of $J = 23/2$ for the $E_x = 3841$ keV state yields the best result. The non-vanishing multipole-mixing ratio $\delta_1 = -0.09(3)$ clearly indicates that the 296-keV transition is parity-conserving. Assuming a non-zero fixed δ_2 value of the 1195-keV transition and a variable δ_1 value of the 296-keV transition, the χ^2 value of the $23/2 \xrightarrow{\delta_1} 21/2 \xrightarrow{\delta_2} 19/2$ hypothesis get larger (i.e. $\delta_2 = \pm 0.05$; $\chi^2 > 2.2$ and $\delta_2 = \pm 0.1$; $\chi^2 > 2.9$). Based on the results of the shell-model calculations presented in Sec. IV B, this observation supports a pure-dipole $E1$ 1195-keV transition which is in line with a change from negative to positive parity.

IV. SHELL MODEL

The extended level schemes of ^{136}Ba and ^{137}Ba are compared with the results of shell-model theory. All

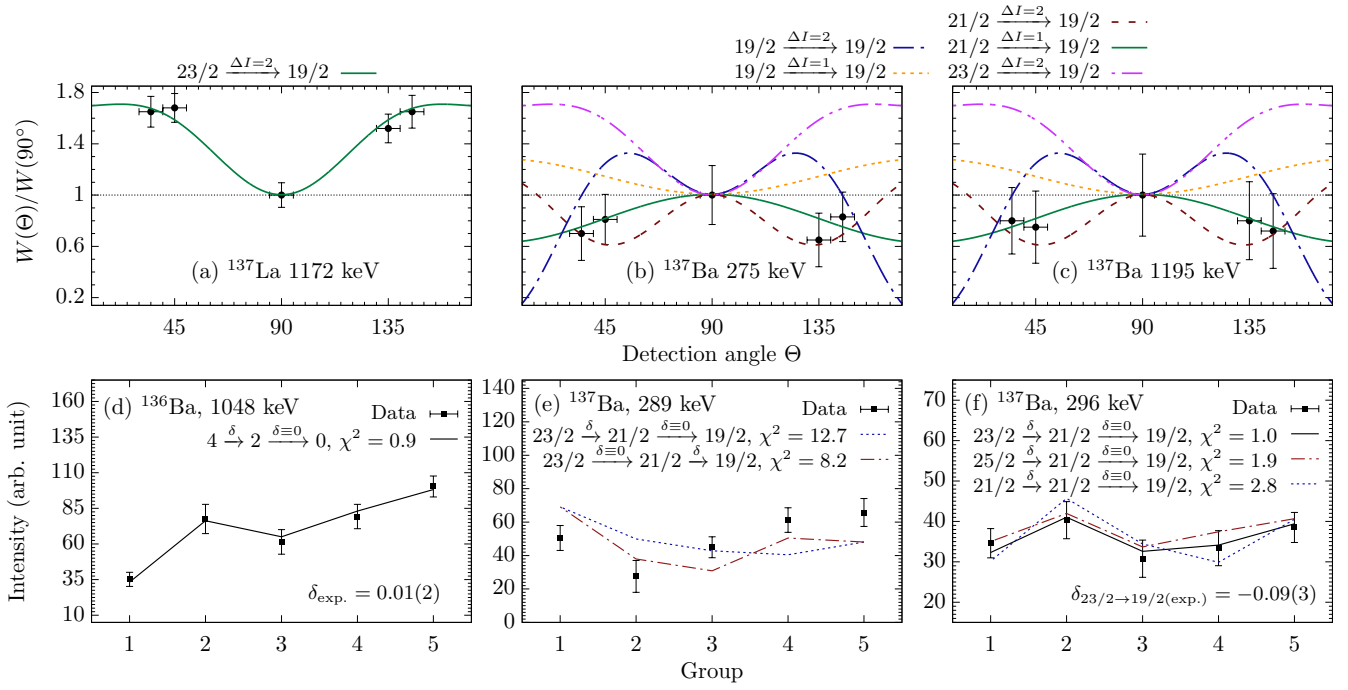


Figure 6. (Color online) Angular distributions of transitions in ^{137}La and ^{137}Ba . Experimental distribution is obtained in the γ -ray spectra, gated on deoriented transitions below the isomers. (a) Benchmark angular distribution of the well-known 1172-keV ($23/2^- \rightarrow 19/2^-$) γ -ray transition in ^{137}La . The pure quadrupole hypothesis is well reproduced with this approach. Angular distribution of (b) 275 and (c) 1195-keV transition, decaying into the $19/2^-$ isomer in ^{137}Ba . Intensities are extracted from $\gamma\gamma$ coincident spectra with a gate on the $15/2^- \rightarrow 11/2^-$ transition. Several pure dipole and quadrupole hypothesis (lines) are plotted. (d) Benchmark $\gamma\gamma$ angular-correlations for the $4_1^+ \rightarrow 2_1^+ \rightarrow 0_1^+$ (1048-818-keV) cascade in ^{136}Ba . Investigation for (e) the 289-275-keV cascade and (f) the 296-1195-keV cascade in ^{137}Ba . Several spin hypotheses are plotted.

696 shell-model calculations were carried out in an untruncated
697 *gdsh* valence space outside doubly-magic ^{100}Sn ,
698 employing the shell-model code NUSHELLX@MSU [60],
699 the massive-parallelization code KSHELL [61], and the
700 ANTOINE shell-model code [62].

701 The first calculation is conducted with the effective in-
702 teraction GCN50:82 [63, 64]. The interaction is derived
703 from a realistic G matrix based on the Bonn-C poten-
704 tial [65]. Empirical monopole corrections to the original
705 G matrix are introduced by fitting different combinations
706 of two-body matrix elements to sets of experimental exci-
707 tation energies from even-even and even-odd semi-magic
708 nuclei.

709 The second calculation is conducted in the framework
710 of the realistic shell model [66, 67], denoted as Realistic
711 SM. Single-particle energies and two-body effective in-
712 teraction are determined from the established CD-Bonn
713 free nucleon-nucleon potential [65] using the $V_{\text{low-}k}$ ap-
714 proach with a cutoff momentum of $\Lambda = 2.6 \text{ fm}^{-1}$, plus
715 the Coulomb force for protons. The effective shell-model
716 Hamiltonian is derived iteratively by means of the many-
717 body perturbation theory in the \hat{Q} -box folded diagram
718 expansion, including all diagrams up to third order in
719 the interaction. More details can be found in Ref. [68].

720 A third calculation is performed utilizing the frame-
721 work of the pair-truncated shell model, denoted as
722 PQM130 (Pairing+QQ+Multipole for mass region 130).

723 The approach leverages a pairing-plus-quadrupole in-
724 teraction that consists of spherical single-particle ener-
725 gies, a monopole-pairing, a quadrupole-pairing, and a
726 quadrupole-quadrupole interaction. The Hamiltonian in
727 each neutron and proton space is diagonalized separately
728 and afterwards the total Hamiltonian is diagonalized in
729 the truncated space. More details on the calculation are
730 given in Refs. [69, 70].

731 Another calculation is carried out with the *jj55pn*
732 Hamiltonian (referred to as the SN100PN interac-
733 tion) [71]. The Hamiltonian consists of four terms cover-
734 ing the neutron-neutron, neutron-proton, proton-proton,
735 and Coulomb repulsion between the protons individu-
736 ally. A renormalized G matrix derived from the CD-Bonn
737 interaction [65] was employed to construct the realistic
738 two-body residual interaction. The proton and neutron
739 single-particle energies are based upon the energy levels
740 in ^{133}Sb and ^{131}Sn .

741 A. ^{136}Ba

742 As a first benchmark for the validity of the shell-
743 model results in the high-spin regime, reduced transition
744 probabilities $B(E2; 10_1^+ \rightarrow 8_1^+)$ are calculated with the
745 GCN50:82, Realistic SM, and SN100PN interactions. Ef-

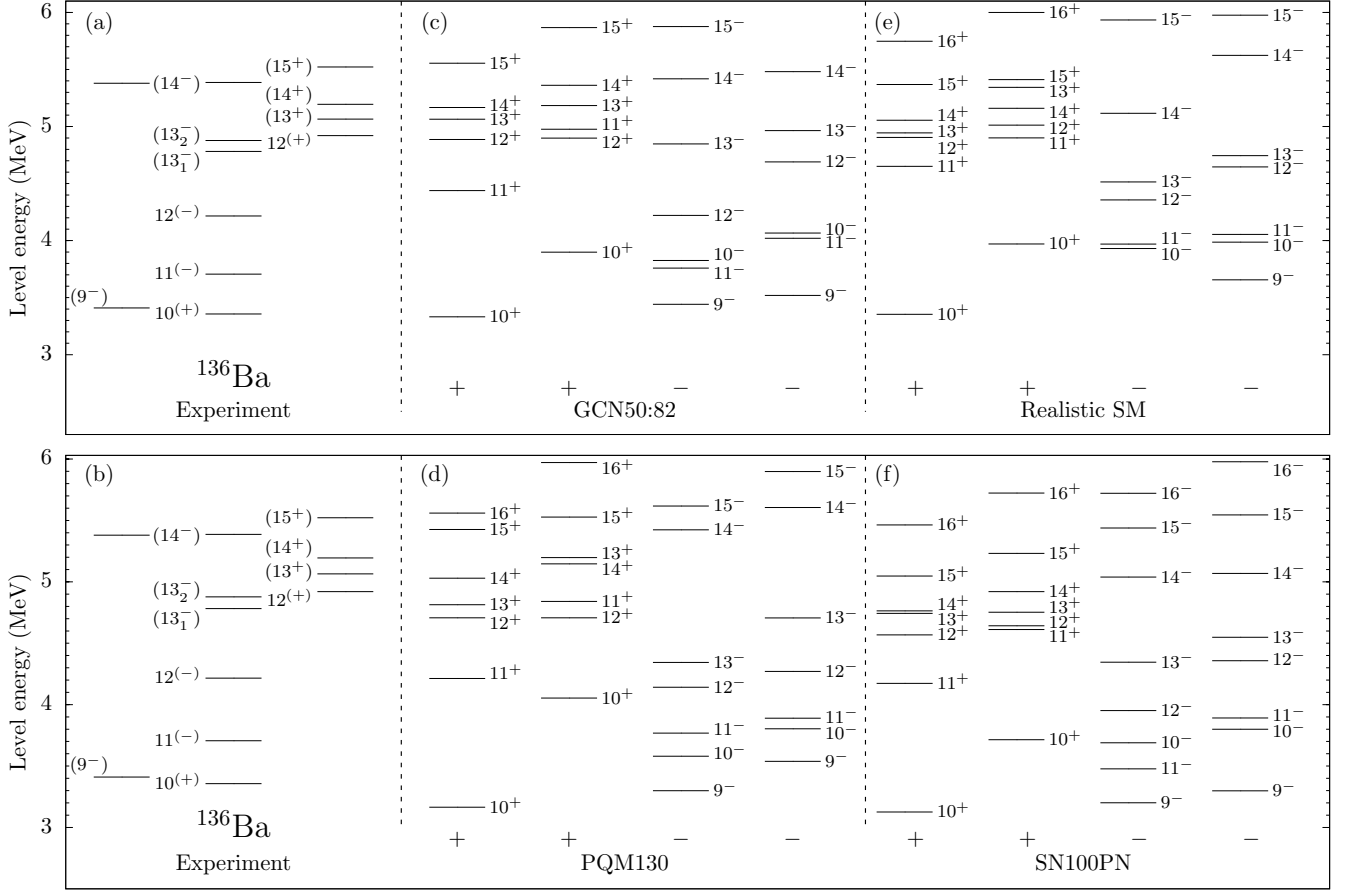


Figure 7. Comparison of experimental energy spectra with the results of shell-model calculations for ^{136}Ba . Only states above the $J^\pi = 10^+$ state are displayed. For clarity, the states are separated into columns for positive- and negative-parity states, as well as for yrast and yrare states. (a)-(b) Experimental energy spectra, shell-model results obtained with (c) GCN50:82, (d) PQM130, (e) Realistic SM and, (f) SN100PN interactions.

fective charges are chosen as $e_\pi = 1.82$ and $e_\nu = 0.82$ in the GCN50:82 and SN100PN interaction, while an effective microscopic $E2$ operator, derived consistently with the effective Hamiltonian, is employed in Realistic SM. The effective charge values are equal to the charges used in a previous study of ^{136}Ba [3].

The calculated $B(E2; 10_1^+ \rightarrow 8_1^+)$ values of $0.81 e^2\text{fm}^4$ (GCN50:82), $0.44 e^2\text{fm}^4$ (SN100PN), and $0.22 e^2\text{fm}^4$ (Realistic SM) are in reasonable agreement with the previously reported experimental values of $0.97(2) e^2\text{fm}^4$ [3] and $0.96(10) e^2\text{fm}^4$ [14]. The agreement between calculated and experimental $B(E2; 10_1^+ \rightarrow 8_1^+)$ value has improved considerably compared to the shell-model calculations conducted in Ref. [3].

Calculated level energies of four shell-model calculations are compared to the experimental levels of ^{136}Ba , as shown in Fig. 7 ((c) GCN50:82; (d) PQM130; (e) Realistic SM; and (f) SN100PN). Since states above the $J^\pi = 10^+$ isomer are subject of this discussion, only these states are displayed. However, also the excitation energies of the yrast states $J^\pi = 2^+, 4^+, 6^+, \text{ and } 8^+$ at excitation energies of $E_x =$

819, 1867, 2207 and 2994 keV are well reproduced. The different shell-model calculations locate the corresponding states at energies of $E_x = 842, 1873, 2195, 3036$ (GCN50:80), $E_x = 1041, 1959, 2297, 3209$ (Realistic SM), $E_x = 814, 1638, 2230, 3109$ (PQM130), and $E_x = 893, 1896, 2083, 2959$ keV (SN100PN).

The calculations predict the $J^\pi = 10_1^+$ state with the $\nu h_{11/2}^{-2}$ configuration at excitation energies of 3332 (GCN), 3354 (Realistic SM), 3164 (PQM130), and 3126 keV (SN100PN), which are in good agreement with the experimentally determined energy of 3357 keV. In particular, the GCN50:82 interaction provides an excellent agreement with the well-known yrast states $J^\pi \leq 10^+$. Larger discrepancies between the calculations emerge in the high-spin regime; e.g. the predictions for the first excited $J^\pi = 12^+$ state differs by 0.5 MeV.

The angular-correlation and angular-distribution measurements in Sec. III A indicated a $J^\pi = 11$ assignment for the 3707-keV state and a pure-dipole character for the 349-keV transition. It is noteworthy that all interactions do not predict a yrast positive-parity state with spin $J > 10$ until approx. 1 MeV above the $J^\pi = 10^+$ state.

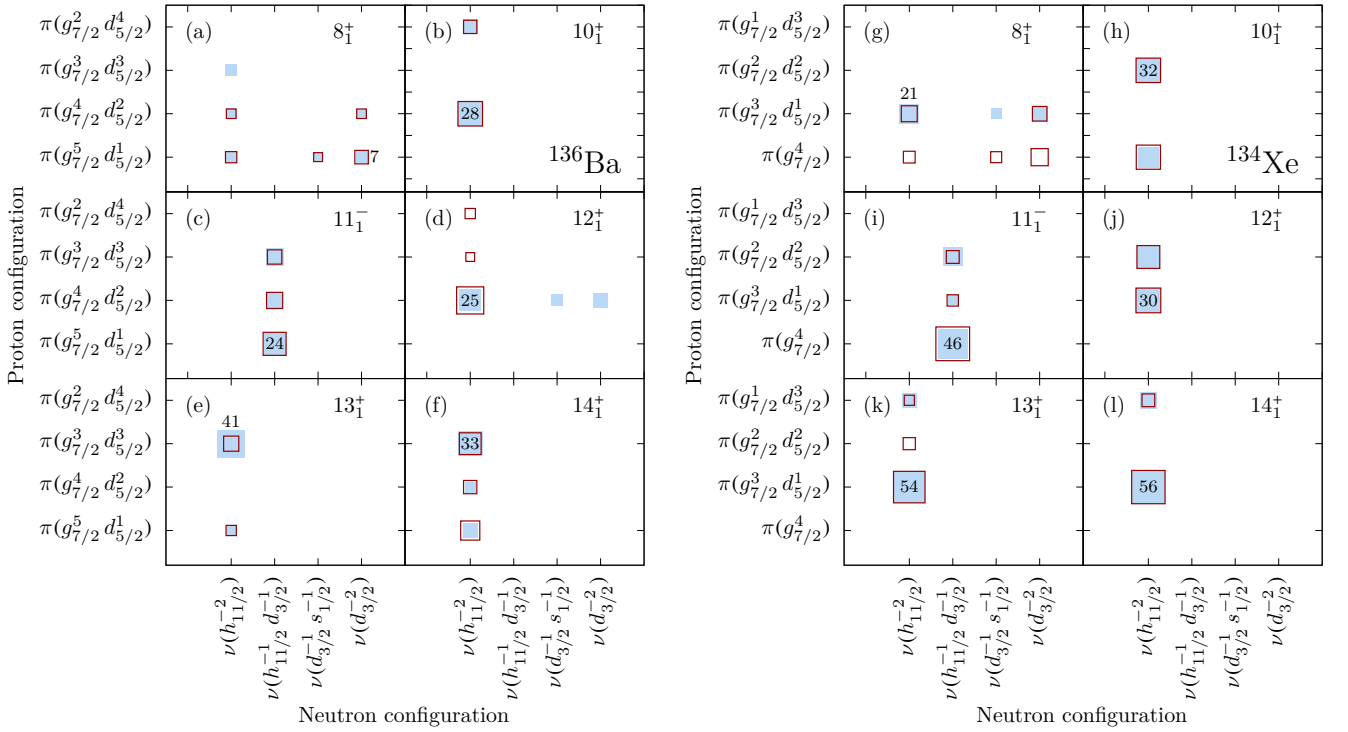


Figure 8. (Color online) Decomposition of the total wave function configuration into its proton and neutron components for several positive- and negative-parity states in (a)-(f) ^{136}Ba and (g)-(l) ^{134}Xe , employing the GCN50:82 (filled blue boxes) and the SN100PN interaction (empty red boxes). Strongest components in the GCN50:82 interaction are labeled with corresponding percentages. The other configurations of both calculations are drawn with areas proportional to their percentages.

790 However, all four interactions yield excited $J^\pi = 10_1^+$,
 791 10_1^- , and 11_1^- states only a few hundred keV above the
 792 isomer. Moreover, $J^\pi = 11^+$ states are coherently pre-
 793 dicted at higher energies than the $J^\pi = 11^-$ states. Ac-
 794 cordingly, a parity-changing $E1$ transition is proposed
 795 and the state at $E_x = 3707$ keV is identified as the
 796 $J^\pi = 11^-$ state, based on these theoretical findings.
 797 Assuming a preceding negative-parity character of this
 798 band, the states at $E_x = 4782$ and $E_x = 4878$ keV, de-
 799 caying parallel into the $J^\pi = 12^-$ 4217 keV state, can
 800 most likely be interpreted as the first and second excited
 801 $J^\pi = 13^-$ states.

802 In the calculations the energy difference between the
 803 $J^\pi = 12_1^+$ and $J^\pi = 10_1^+$ state amount to 1555
 804 (GCN50:82), 1551 (Realistic SM), 1543 (PQM130), and
 805 1442 keV (SN100PN). The calculated values are in good
 806 agreement with the experimentally observed energy dif-
 807 ference of 1562 keV between the $J^\pi = 10_1^+$ and the
 808 $E_x = 4920$ keV state. In the aforementioned discus-
 809 sion of Fig. 5(f) a pure-dipole character of the 1214-keV
 810 transition was confirmed, which suggests a parity change.
 811 Combining this experimental result with the shell-model
 812 results, the $E_x = 4920$ keV state is clearly assigned to
 813 $J^\pi = 12^+$.

814 On top of the $E_x = 4921$ keV state, a low-energy 328-
 815 130-144-keV cascade is observed. The calculated transi-
 816 tion energies in the $15^+ \rightarrow 14^+ \rightarrow 13^+ \rightarrow 12^+$ cascade

817 are 388-103-177 (GCN), 314-111-39 (Realistic SM), 397-
 818 215-106 (PQM130), and 233-111-135 keV (SN100PN), re-
 819 spectively. According to the good agreement between
 820 calculated and experimental energy differences, the 328-
 821 130-144-keV cascade can most likely be attributed to
 822 the $15^+ \rightarrow 14^+ \rightarrow 13^+ \rightarrow 12^+$ sequence. Shell-model
 823 calculations suggest a dominant $M1$ character for this
 824 band; i.e. GCN50:82 predicts multipole-mixing ratios of
 825 $\delta_{15 \rightarrow 14} = -0.05$, $\delta_{14 \rightarrow 13} = -0.01$, and $\delta_{13 \rightarrow 12} = -0.02$
 826 which are very similar to the values calculated with
 827 SN100PN. In the calculations $J^\pi = 9^-$ states are pre-
 828 dicted slightly above the $J^\pi = 10^+$ isomer. In accordance
 829 with the angular-correlation measurement, a tentative
 830 spin assignment of $J^\pi = (9^-)$ for the $E_x = 3410$ -keV
 831 state is made.

832 The shell-model results provide insight into the struc-
 833 ture of the levels built on top of the isomeric $J^\pi = 10_1^+$
 834 state. The nuclear structure of ^{136}Ba and the $-2p$ iso-
 835 tone ^{134}Xe have similar characteristics. Figure 8 shows a
 836 detailed decomposition of several states into their proton
 837 and neutron configurations in (a)-(f) ^{136}Ba and (g)-(l)
 838 ^{134}Xe computed with GCN50:82 (filled blue boxes) and
 839 SN100PN (empty red boxes). The decomposition of the
 840 total angular momentum of states in ^{134}Xe and ^{136}Ba are
 841 presented in Figs. 9(a)-(l) indicating which nucleon pairs
 842 are broken to obtain the total angular momentum of the
 843 calculated states.

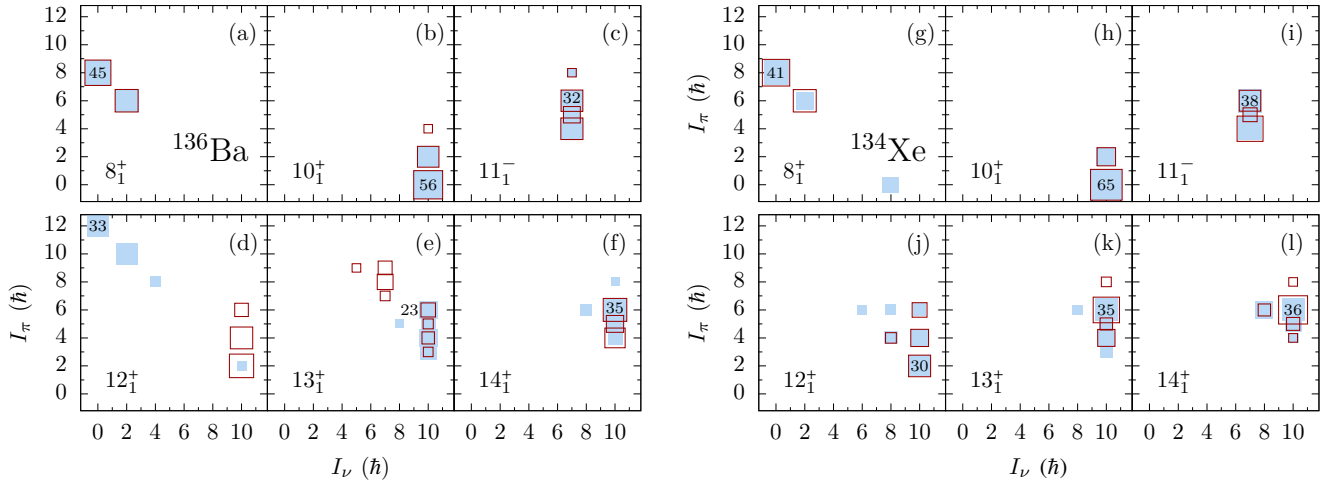


Figure 9. (Color online) Decomposition of the total angular momentum of selected states of (a)-(f) ^{136}Ba and (g)-(l) ^{134}Xe , using the GCN50:82 interaction (filled blue boxes) and the SN100PN interaction (empty red boxes) into their proton and neutron spins.

844 Although more fragmented in ^{136}Ba , the configurations
 845 resemble the ones in ^{134}Xe . In the different positive- and
 846 negative-parity states, protons are easily redistributed
 847 from $g_{7/2}$ to $d_{5/2}$, i.e., these orbitals are energetically
 848 close together.

849 The configurations of the $J^\pi = 8_1^+$ state in ^{134}Xe and
 850 ^{136}Ba are predicted to be highly fragmented in both
 851 calculations, as displayed in Figs. 8(a) and 8(g). In
 852 ^{134}Xe , the four valence protons mainly occupy the $\pi(g_{7/2}^4)$
 853 and the $\pi(g_{7/2}^3 d_{5/2}^1)$ configuration. The total angular
 854 momentum of the $J^\pi = 8^+$ state is mainly generated
 855 from these configurations in the proton space, as visible
 856 in Fig. 9(g). Excitations into the proton $h_{11/2}$ orbital
 857 can be neglected ($< 2\%$). Using GCN50:82, the
 858 neutron configurations $\nu h_{11/2}^{-2}$, $\nu(h_{11/2}^{-1} s_{1/2}^{-1})$, and $\nu d_{3/2}^{-2}$
 859 account for 20%, 10%, and 16% of the overall configura-
 860 tion in the $J^\pi = 8_1^+$ state in ^{136}Ba , respectively. In
 861 the Realistic-SM calculation main configurations are cou-
 862 plings of the $\pi(g_{7/2}^5 d_{5/2}^1)$ proton configuration to (17%)
 863 $\nu d_{3/2}^{-2}$ and (15%) $\nu h_{11/2}^{-2}$, which is in good agreement with
 864 the results of the GCN50:82 and SN100PN calculations.
 865 Similarly to ^{134}Xe , the $J^\pi = 8^+$ state in ^{136}Ba is domi-
 866 nated by proton spins of (45%) $I_\pi = 8$ and (37%) $I_\pi = 6$,
 867 as displayed in Fig. 9(a).

868 The wave function of the isomeric $J^\pi = 10_1^+$ state in
 869 ^{136}Ba is dominated by the neutron $\nu(h_{11/2}^{-2})$ configura-
 870 tion with spins of 56% $\nu_{10^+} \otimes \pi_{0^+}$ and 30% $\nu_{10^+} \otimes \pi_{2^+}$.
 871 A major $\nu(h_{11/2}^{-2})$ configuration for the $J^\pi = 10_1^+$ state
 872 is also in accordance with the SN100PN and Realistic
 873 SM calculations. Significant deviations between the cal-
 874 culations arise for the $J^\pi = 12_1^+$ state in ^{136}Ba . The
 875 decomposition matrix of the $J^\pi = 12_1^+$ bandhead of the
 876 positive-parity band computed by the GCN50:82 interac-
 877 tion, displayed in Fig. 8(d), shows an additional occupa-
 878 tion of the neutron $d_{3/2}$ and $s_{1/2}$ orbital, which reduces

879 the occupation of the $\nu(h_{11/2}^{-2})$ configuration. A declin-
 880 ing impact of the $\nu(h_{11/2}^{-2})$ configuration of the $J^\pi = 12_1^+$
 881 state in ^{136}Ba is also predicted by the Realistic SM where
 882 $\pi(g_{7/2}^5 h_{11/2}^1) \otimes \nu(d_{3/2}^{-1} h_{11/2}^{-1})$ is computed as main configu-
 883 ration with a probability of 51%. However, the SN100PN
 884 interaction does not predict a change of neutron occupa-
 885 tion between the $J^\pi = 10_1^+$ and $J^\pi = 12_1^+$ states. Such
 886 discrepancies between both calculations are not observed
 887 for states in ^{134}Xe .

888 The differences in the predicted structure of the $J^\pi =$
 889 12^+ state is mirrored in the spin composition, as visible
 890 in Fig. 9(d). While the SN100PN interaction predicts a
 891 dominant neutron spin of (91%) $I_\nu = 10^+$, the GCN50:82
 892 predicts this fully-aligned neutron-spin configuration to
 893 be insignificant (7%). Instead, major contributions stem
 894 from $\pi_{12^+} \otimes \nu_{0^+}$ and $\pi_{10^+} \otimes \nu_{2^+}$. The proton spin is gen-
 895 erated dominantly by the $\pi(g_{7/2}^4 d_{5/2}^2)$ configuration with
 896 a maximum spin contribution of $I_\pi = 12$. The proton
 897 $h_{11/2}$ orbital does not contribute considerably ($< 2\%$) to
 898 the configuration of the $J^\pi = 12^+$ state using GCN50:82.

899 Going to higher spins along the positive-parity band,
 900 a strong $\nu(h_{11/2}^{-2})$ contribution returns to prevail for
 901 $J^\pi \geq 13_1^+$ states in the GCN50:82 calculation. Con-
 902 figurations including the neutron $d_{3/2}$ orbital become
 903 negligibly small in the GCN50:82 and SN100PN inter-
 904 actions. In contrast, the leading neutron configuration of
 905 the negative-parity states with $J^\pi > 10_1^-$ is $\nu(h_{11/2}^{-1} d_{3/2}^{-1})$.
 906 The neutron $\nu(h_{11/2}^{-2})$ configuration nearly vanishes in the
 907 decomposition of the negative-parity states.

908 The role of the different proton and neutron orbitals is
 909 further scrutinized by investigating the evolution of aver-
 910 erage occupation numbers of neutrons in the *gdsh* model
 911 space for several high-spin states in $N = 80$ isotones, as
 912 listed in Tab. II. In all even-mass isotones from ^{134}Xe to

913 ^{138}Ce , the average occupation of the neutron $h_{11/2}$ orbital
 914 for the $J^\pi = 10^+$ states is $N_\nu \approx 10$, indicating a two-
 915 neutron $\nu h_{11/2}^{-2}$ configuration. However, in the GCN50:82
 916 and Realistic SM interactions, the $\nu d_{3/2}$ orbital is gain-
 917 ing significance for the $J^\pi = 11_1^-$ and 12_1^+ states from
 918 ^{136}Ba onwards. Furthermore, both states have only one
 919 neutron hole in the $\nu h_{11/2}$ orbital ($N_\nu \approx 11$). For com-
 920 pleteness, the corresponding average occupation of the
 921 neutron $d_{3/2}$, $s_{1/2}$, and $h_{11/2}$ orbitals in the Realistic
 922 SM calculation have values of 3.12, 1.99, 11.01 for the
 923 $J^\pi = 11_1^-$ state and 3.23, 1.87, 11.00 for the $J^\pi = 12_1^+$
 924 state, respectively. Accordingly, proton configurations
 925 are vital to generate the spin, which is consistent with
 926 the results presented in Figs. 8(c)-(d). Hence, the con-
 927 figuration of the $J^\pi = 12_1^+$ state in ^{136}Ba , calculated by
 928 GCN50:82 and Realistic SM, mirrors rather the configu-
 929 ration of the $J^\pi = 11_1^-$ state than that of the $J^\pi = 10_1^+$
 930 state, which supports a decay of the $J^\pi = 12_1^+$ state into
 931 the $J^\pi = 11_1^-$ state.

932 The dominating proton configuration of the yrast $J^\pi =$
 933 8^+ state causes the isomeric character of the two-neutron
 934 hole $J^\pi = 10_1^+$ state [3]. In a similar way, the unobserved
 935 $12^+ \rightarrow 10^+$ transition can be understood microscopically.
 936 ^{136}Ba is the lowest-mass isotone along the $N = 80$ chain
 937 in which an angular momentum of $J = 12$ can be gener-
 938 ated exclusively from protons in the $g_{7/2}$ and $d_{5/2}$ orbitals
 939 (i.e. $\pi(g_{7/2}^4 d_{5/2}^2)$). The dominating proton configuration
 940 of the $J^\pi = 12^+$ state, as calculated by the GCN50:82
 941 interaction and the Realistic-SM interaction, hinders a
 942 decay into the two-neutron hole $J^\pi = 10^+$ state. Calcul-
 943 ated reduced transition probabilities $B(E2; 12^+ \rightarrow 10^+)$
 944 underpin the reliability of the GCN50:82 and Realistic-
 945 SM interaction. Corresponding values are compatible in
 946 ^{134}Xe ($215 e^2\text{fm}^4$ with GCN50:82 and $222 e^2\text{fm}^4$ with
 947 SN100PN), while they differ significantly in ^{136}Ba : The
 948 larger proton component in the $J^\pi = 12^+$ state causes
 949 a lower $B(E2; 12^+ \rightarrow 10^+)$ value of $62 e^2\text{fm}^4$ in the
 950 GCN50:82 and of $3 e^2\text{fm}^4$ in the Realistic-SM calcula-
 951 tion, compared to $B(E2; 12^+ \rightarrow 10^+) = 375 e^2\text{fm}^4$ using
 952 SN100PN. The low $B(E2; 12^+ \rightarrow 10^+)$ values in the
 953 GCN50:82 and Realistic-SM calculations is in agreement
 954 with the experimentally unobservability of this transi-
 955 tion.

956 Interestingly, adding two protons to ^{136}Ba , the occu-
 957 pation number of $N_\nu \approx 11$ for the neutron $h_{11/2}$ orbital
 958 in Tab. II indicates that the SN100PN interaction pre-
 959 dicted an emerging proton component for the $J^\pi = 12^+$
 960 state in ^{138}Ce .

961 B. ^{137}Ba

962 Calculated level energies for states above the $J =$
 963 $19/2^-$ isomer in ^{137}Ba ((c) GCN50:82; (d) PQM130; (e)
 964 Realistic SM and (f) SN100PN), are compared to exper-
 965 imental level energies in Fig. 10. The pivotal $J = 11/2^-$
 966 neutron-hole isomer at $E_x = 662$ keV is predicted at

Table II. Average neutron occupation numbers in each single-
 particle orbit of the $gdsh$ model space for observed high-spin
 states in ^{134}Xe , ^{136}Ba , and ^{138}Ce using the GCN50:82 and
 SN100PN interaction.

Isotope	J^π	$g_{7/2}$	$d_{5/2}$	$d_{3/2}$	$s_{1/2}$	$h_{11/2}$
GCN50:81						
^{134}Xe	10_1^+	8.00	6.00	4.00	2.00	10.00
	11_1^-	7.97	5.97	3.06	1.99	11.00
	12_1^+	8.00	6.00	4.00	2.00	10.00
^{136}Ba	10_1^+	7.99	5.99	4.00	2.00	10.03
	11_1^-	7.96	5.96	3.09	1.99	11.00
	12_1^+	7.87	5.86	3.57	1.79	10.91
^{138}Ce	10_1^+	7.98	5.98	3.99	2.00	10.05
	11_1^-	7.94	5.95	3.11	1.99	11.00
	12_1^+	7.94	5.96	3.16	1.94	11.00
SN100PN						
^{134}Xe	10_1^+	8.00	6.00	4.00	2.00	10.00
	11_1^-	7.98	5.96	3.07	1.99	11.00
	12_1^+	8.00	6.00	4.00	2.00	10.00
^{136}Ba	10_1^+	8.00	6.00	4.00	2.00	10.00
	11_1^-	7.97	5.95	3.11	1.98	11.00
	12_1^+	8.00	5.99	3.99	2.00	10.03
^{138}Ce	10_1^+	7.99	5.99	4.00	2.00	10.02
	11_1^-	7.95	5.93	3.13	1.99	11.00
	12_1^+	7.96	5.94	3.21	1.89	11.00

967 excitation energies of 534 (GCN50:82), 643 (Realistic
 968 SM), 692 (PQM130), and 478 keV (SN100PN). The shell-
 969 model calculations compute the 120-1567-keV cascade
 970 to have γ -ray energies of 285-1396 (GCN50:82), 412-
 971 1491 (PQM130), and 231-1396 keV (SN100PN). Going
 972 to higher spins, the energy differences in the four calcu-
 973 lations between states of same spin and parity amount
 974 for up to 1 MeV.

975 In the calculated excitation pattern, the $J^\pi = 21/2_1^-$
 976 states emerge at 240 (GCN50:82), 195 (Realistic SM),
 977 234 (PQM130), and 220 keV (SN100PN) above the $J^\pi =$
 978 $19/2_1^-$ states. Moreover, $J^\pi = 23/2_1^-$ states are predicted
 979 684 (GCN50:82), 465 (Realistic SM), 100 (PQM130), and
 980 425 keV (SN100PN) higher in excitation energy with re-
 981 spect to the $J^\pi = 21/2_1^-$ state. In accordance with
 982 the results of $\gamma\gamma$ angular-correlation measurements (see
 983 Fig. 6(b) and (e)), which confirmed mixed $M1/E2$ 289-
 984 and 275-keV transitions and therefore a parity-conserving
 985 289-275-keV cascade, the $E_x = 2624$ - and $E_x = 2913$ -keV
 986 states are identified as the first excited $J^\pi = 21/2^-$ and
 987 $23/2^-$ states, respectively.

988 Going to higher spins along the negative-parity band,
 989 in particular GCN50:82 tend to group pairs of yrast spins
 990 ($J^\pi = 25/2^-$, $27/2^-$) and ($J^\pi = 29/2^-$, $31/2^-$). Both
 991 groups are separated by a larger energy gap compared to
 992 the energy gaps between both states within the group.

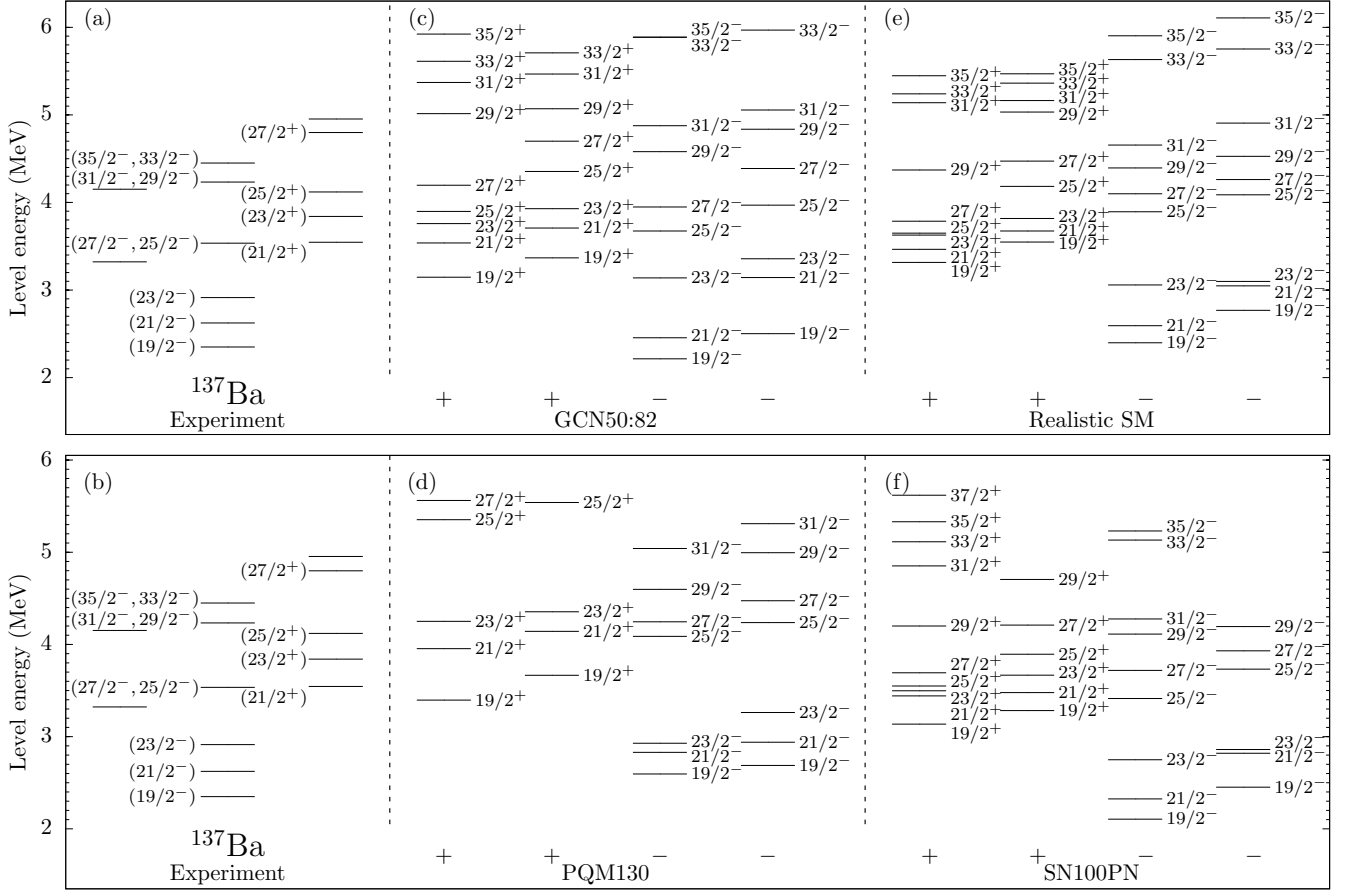


Figure 10. Comparison of experimental energy spectra with the results of shell-model calculations for ^{137}Ba . Only states above the $J^\pi = 19/2^-$ state are displayed. For clarity, the states are separated into columns for positive- and negative-parity states, as well as for yrast and yrare excited states. (a)-(b) Experimental energy spectra, shell-model results obtained with (c) GCN50:82, (d) PQM130, (e) Realistic SM, and (f) SN100PN interactions.

993 This observation associates the $E_x = 3611$ -keV state with 1015 states. Consequently, a spin of $J^\pi = 23/2^+$ for the
 994 $J^\pi = (25/2^-, 27/2^-)$ and the $E_x = 4233$ -keV state with 1016 $E_x = 3841$ keV state is in agreement with shell-model
 995 $J^\pi = (29/2^-, 31/2^-)$. 1017 calculations.

996 Similar to the $E_x = 2624$ -keV state, also the spin 1018 Due to the large density of predicted states above
 997 of the $E_x = 3545$ -keV state is measured to be of spin 1019 4 MeV, no unambiguous assignment for the $E_x = 4120$ -
 998 $J = 21/2$ (see Fig. 6(c)). Positive-parity states of similar 1020 and 4799-keV states is possible. Since both states do not
 999 spin ($J \geq 19/2_1^+$) are calculated to appear at higher 1021 exhibit decay branches into the $J^\pi = 19/2^-$ or $21/2^-$
 1000 excitation energy than the $J^\pi = 19/2_1^-$ state. The 1022 state, they have most likely spins $J > 23/2$. By a similar
 1001 energy difference between the $J^\pi = 19/2_1^-$ and $21/2_1^+$ 1023 argument the 3322 and 4152 keV states are interpreted to
 1002 states is predicted to be 1323 (GCN50:82), 1067 (Real- 1024 have a spin of $J > 21/2$. Otherwise, they would directly
 1003 istic SM), 1360 (PQM130), and 1337 keV (SN100PN). 1025 decay to the $J^\pi = 19/2^-$ state.

1004 In accordance with the experimental results obtained in 1026 The theoretical wave functions of ^{137}Ba are not as frag-
 1005 the angular-correlation and angular-distribution investi- 1027 mented as in ^{136}Ba . The decomposition of the total angu-
 1006 gations (see Fig. 6(c) and (f)), the state at $E_x = 3545$ keV 1028 lar momentum $I = I_\pi \otimes I_\nu$ into its proton and neutron
 1007 is interpreted as the first excited $J^\pi = 21/2^+$ state and, 1029 components for the $J^\pi = 19/2_1^-, 21/2_1^+$ and $23/2_1^+$ states
 1008 thus, as the bandhead of the positive-parity band. 1030 in ^{137}Ba predicted by the GCN50:82 and SN100PN is pre-
 1009 Moreover, assuming a $J = 23/2$ assignment for the 1031 sented in Fig. 11. Table III shows the calculated average
 1010 3841-keV state, the multipole-mixing ratio of the 296- 1032 neutron occupation numbers of each orbital in the $gdsh$
 1011 keV transition is measured as $\delta = -0.09(3)$ which sug- 1033 model space. For GCN50:82, the $J^\pi = 19/2_1^-$ isomer con-
 1012 gests that the 3841-keV state has the same parity as the 1034 sists mainly (29%) of the $\nu h_{11/2}^{-1} \otimes \pi(g_{7/2}^5 d_{5/2}^1)$, 21% of the
 1013 3545-keV state (see Fig. 6(f)). Excited $J = 23/2_1^+$ states 1035 $\nu h_{11/2}^{-1} \otimes \pi(g_{7/2}^3 d_{5/2}^3)$, and 13% of the $\nu h_{11/2}^{-1} \otimes \pi(g_{7/2}^4 d_{5/2}^2)$
 1014 are calculated 152 to 453 keV above the $J = 21/2_1^+$

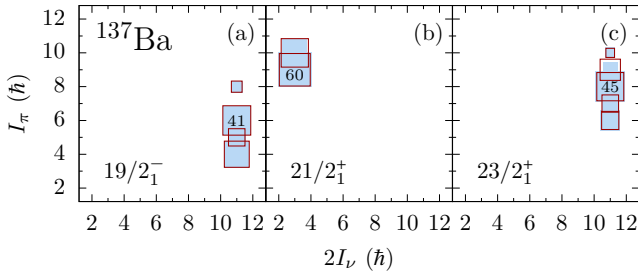


Figure 11. (Color online) Decomposition of the total angular momentum of selected states of ^{137}Ba , using the GCN50:82 interaction (filled blue boxes) and the SN100PN interaction (empty red boxes) into their proton and neutron spins $I_\pi \otimes I_\nu$.

Table III. Average neutron occupation numbers in each single-particle orbit of the *gdsh* model space in ^{137}Ba , calculated using the GCN50:82 and SN100PN interaction.

J^π	$g_{7/2}$	$d_{5/2}$	$d_{3/2}$	$s_{1/2}$	$h_{11/2}$
GCN50:82					
$19/2_1^-$	8.00	6.00	4.00	2.00	11.00
$21/2_1^+$	7.98	5.98	3.07	1.98	11.99
$23/2_1^+$	8.00	6.00	4.00	2.00	11.00
SN100PN					
$19/2_1^-$	8.00	6.00	4.00	2.00	11.00
$21/2_1^+$	7.99	5.98	3.08	1.96	12.00
$23/2_1^+$	8.00	6.00	4.00	2.00	11.00

configuration. The dominating neutron-hole $\nu h_{11/2}^{-1}$ configuration is also visible in the average occupation numbers with an occupation of $N_\nu \approx 11$ in the neutron $h_{11/2}$ orbital. Also the SN100PN and the Realistic-SM calculation predict a strong neutron-hole $\nu h_{11/2}^{-1}$ configuration for the $J^\pi = 19/2_1^-$ state. Couplings of this configuration to proton configurations with spins of 4^+ (33%), 5^+ (16%), and 6^+ (41%) contribute to the $J^\pi = 19/2_1^-$ state. Also for the $J^\pi = 21/2^+$, $J^\pi = 23/2^+$, and higher-lying negative-parity states the neutron $\nu h_{11/2}^{-1}$ configuration dominates.

The positive-parity bands in ^{136}Ba and ^{137}Ba have mirroring structures. In each nucleus, positive-parity bands are connected via a high-energy (≈ 1.2 MeV) transition to the negative-parity band. Like the $J^\pi = 12^+$ bandhead in ^{136}Ba , the $J^\pi = 21/2^+$ bandhead in ^{137}Ba shows a smaller degree of $\nu d_{3/2}$ occupation than for the $J^\pi = 19/2^-$ state. The $\nu h_{11/2}$ orbital becomes fully occupied, as calculated by GCN50:82, Realistic SM, and SN100PN (see Tab. III). GCN50:82 predicts a mixture of (67%) $\nu d_{3/2}^{-1} \otimes \pi(g_{7/2}^5 d_{5/2}^1)$ and (11%) $\nu d_{3/2}^{-1} \otimes \pi(g_{7/2}^3 d_{5/2}^3)$ with dominating proton-spin components of $I_\pi = 9^+$ and 10^+ coupled to neutron spin $I_\nu = 3/2^+$ in the $J^\pi = 21/2^+$ state in ^{137}Ba . All three interactions predict

a similar structure for the $J^\pi = 21/2^+$ state. From the second excited state in this band onwards ($J^\pi \geq 23/2_1^+$), the valence neutron hole, is mainly occupying the $\nu h_{11/2}$ orbital. As a consequence a dominating neutron spin of $I_\nu = 11/2^-$ returns to prevail, as shown in Fig. 11(c). According to the distinct similarities of the configurations, the $J^\pi = 21/2^+$ bandhead in ^{137}Ba can be interpreted as the configuration of the $J^\pi = 12^+$ state in ^{136}Ba coupled to a $\nu h_{11/2}$ neutron hole. Interestingly, in ^{137}Ba SN100PN is able to describe the predominant proton character of the $J^\pi = 21/2^+$ state, which is the $J^\pi = 12^+$ state analogon in the even-even core ^{136}Ba , to which a single neutron is coupled, but it is unable to describe the proton structure of the $J^\pi = 12^+$ state in ^{136}Ba .

V. CONCLUSIONS

In summary, four experiments employing two $^9\text{Be} + ^{130}\text{Te}$ and one $^{11}\text{B} + ^{130}\text{Te}$ fusion-evaporation reactions as well as the $^{136}\text{Xe} + ^{238}\text{U}$ multinucleon-transfer reaction were used to investigate high-spin states above the $J^\pi = 10^+$ isomer in ^{136}Ba and above the $J^\pi = 19/2^-$ isomer in ^{137}Ba . The level scheme of ^{136}Ba was revised, incorporating nine new states and transitions. Proper spin, and multipolarity assignments were determined by γ -ray angular distribution measurements and $\gamma\gamma$ coincidence relations. The $E_x = 4920$ -keV state is identified as the $J^\pi = 12^+$ state. The high-spin regime of ^{136}Ba differs significantly from the lower mass isotones.

While the high-spin regimes of both ^{132}Te and ^{134}Xe exhibit high-energy $12^+ \rightarrow 10^+$ yrast transitions, no such transition is observed in ^{136}Ba . Instead the $J^\pi = 10^+$ isomer is fed by a $J^\pi = 11^-$ state. This disruption in the nuclear structure along the $N = 80$ isotones is explained by a dominant proton configuration of the $J^\pi = 12^+$ state in ^{136}Ba . While the $J^\pi = 10^+$ isomer consists mainly of neutron configurations, a pure proton configuration for the $J^\pi = 12^+$ state and the interrupting $J^\pi = 11^-$ state is energetically favorable compared to the continuation via a $\nu h_{11/2}$ configuration. The configuration of the $J^\pi = 12^+$ state mirrors the structure of the $J^\pi = 8^+$ state below the isomer. ^{136}Ba is the first isotone along $N = 80$ for which a combined proton alignment in the $g_{7/2}$ and $d_{5/2}$ orbitals can form a spin of $J = 12$. Corresponding shell-model calculations yield ambiguous results. Only the SN100PN interaction predicts a predominant neutron character of the $J^\pi = 12^+$ state, while GCN50:82 and Realistic SM exhibit the emerging proton configuration. In previous publications, it was found that the proton-neutron part of the SN100PN interaction falls short to reproduce several nuclear-structure features in the mass region. SN100PN could not reproduce backbending in the high-spin regime of ^{131}Xe [72] and the decay features of isomeric states in ^{135}Xe and ^{137}Ba [22]. Similar conclusions on the monopole part were also discussed in Ref. [73]. In the present study, it is worthy of

attention that only interactions with improved and corrected monopole parts, i.e. GCN50:82 and Realistic SM, reproduce the non-observation of the $12^+ \rightarrow 10^+$ transition by the different structure of these two levels.

In ^{137}Ba spins above the $J^\pi = 19/2^-$ isomer at $E_x = 2350$ keV were measured for the first time. The $E_x = 3545$ -keV state is proposed to be the bandhead of the positive-parity band, which is explained as the coupling of the aforementioned $J^\pi = 12^+$ state of the even-even core ^{136}Ba and a neutron. The identification of the high-spin structures complete the systematics for $N = 80$ and $N = 81$ isotones in the vicinity of the $N = 82$ shell closure. In future, measurements of lifetimes and g factors that serve as sensitive probes for nucleon alignment should be performed to independently confirm the proposed proton character of the positive-parity bandheads in ^{136}Ba and ^{137}Ba .

press our thanks to Dr. Eri Teruya and Prof. Dr. Naotaka Yoshinaga from Saitama University, Japan, for providing the results of their shell-model calculation with the PQM130 interaction. The research leading to these results has received funding from the German BMBF under contract No. 05P15PKFN9 TP1 and 05P18PKFN9 TP1, from the European Union Seventh Framework Programme FP7/2007-2013 under Grant Agreement No. 262010 - ENSAR, from the Spanish Ministerio de Ciencia e Innovación under contract FPA2011-29854-C04, from the Spanish Ministerio de Economía y Competitividad under contract FPA2014-57196-C5, and from the U.K. Science and Technology Facilities Council (STFC). L.K. and A.V. thank the Bonn-Cologne Graduate School of Physics and Astronomy (BCGS) for financial support. One of the authors (A. Gadea) has been supported by the Generalitat Valenciana, Spain, under the grant PROM-ETE0II/2014/019 and EU under the FEDER program.

ACKNOWLEDGMENTS

We thank the IKP FN Tandem accelerator team for the support during the experiment. Furthermore, we ex-

-
- [1] B. Fogelberg, K. Heyde, and J. Sau, “Energy levels and transition probabilities in ^{130}Sn ,” *Nucl. Phys. A* **352**, 157 – 180 (1981).
- [2] J. Genevey, J. A. Pinston, C. Foin, M. Rejmund, R. F. Casten, H. Faust, and S. Oberstedt, “Conversion electron measurements of isomeric transitions in $^{130,132}\text{Te}$ and ^{134}Xe ,” *Phys. Rev. C* **63**, 054315 (2001).
- [3] J. J. Valiente-Dobón, P. H. Regan, C. Wheldon, C. Y. Wu, N. Yoshinaga, K. Higashiyama, J. F. Smith, D. Cline, R. S. Chakravarthy, R. Chapman, M. Cromaz, P. Fallon, S. J. Freeman, A. Gørgen, W. Gelletly, A. Hayes, H. Hua, S. D. Langdown, I. Y. Lee, X. Liang, A. O. Macchiavelli, C. J. Pearson, Zs. Podolyák, G. Sletten, R. Teng, D. Ward, D. D. Warner, and A. D. Yamamoto, “ ^{136}Ba studied via deep-inelastic collisions: Identification of the $(\nu h_{11/2})_{10^+}^{-2}$ isomer,” *Phys. Rev. C* **69**, 024316 (2004).
- [4] J. Ludziejewski, J. Bialkowski, Z. Haratym, L-E. de Geer, A. Kerek, and J. Kozyczkowski, “The life-time measurements of some high-spin states in the $^{138,139}\text{Ce}$ and $^{141,142}\text{Nd}$ nuclei,” *Phys. Scr.* **14**, 133 (1976).
- [5] J. C. Merdinger, F. A. Beck, E. Bozek, T. Byrski, C. Gehringer, Y. Schutz, and J. P. Vivien, “Magnetic moments of the $I^\pi = 10^+$ isomers in Ce and Nd $N = 80$ isotones,” *Nucl. Phys. A* **346**, 281 – 284 (1980).
- [6] M. Lach, J. Styczen, R. Julin, M. Piiparinen, H. Beuscher, P. Kleinheinz, and J. Blomqvist, “The 10^+ states of $\nu h_{11/2}^{-2}$ and $\pi h_{11/2}^2$ character in the $N = 80$ isotones ^{144}Gd and ^{142}Sm ,” *Z. Phys. A – Atoms and Nuclei* **319**, 235–236 (1984).
- [7] H. A. Roth, S. E. Arnell, D. Foltescu, Ö. Skeppstedt, J. Blomqvist, G. de Angelis, D. Bazzacco, and S. Lunardi, “Yrast level structure of the neutron-deficient $N = 80$ isotones ^{146}Dy , ^{147}Ho and ^{148}Er up to high-spin values,” *Eur. Phys. J. A* **10**, 275–287 (2001).
- [8] S. Biswas, R. Palit, A. Navin, M. Rejmund, A. Bisoi, M. Saha Sarkar, S. Sarkar, S. Bhattacharyya, D. C. Biswas, M. Caamaño, M. P. Carpenter, D. Choudhury, E. Clément, L. S. Danu, O. Delaune, F. Farget, G. de France, S. S. Hota, B. Jacquot, A. Lemasson, S. Mukhopadhyay, V. Nanal, R. G. Pillay, S. Saha, J. Sethi, Purnima Singh, P. C. Srivastava, and S. K. Tandel, “Structure of $^{132}\text{Te}_{80}$: The two-particle and two-hole spectrum of $^{132}\text{Sn}_{82}$,” *Phys. Rev. C* **93**, 034324 (2016).
- [9] A. Vogt, B. Birkenbach, P. Reiter, A. Blazhev, M. Siciliano, J. J. Valiente-Dobón, C. Wheldon, D. Bazzacco, M. Bowry, A. Bracco, B. Bruyneel, R. S. Chakravarthy, R. Chapman, D. Cline, L. Corradi, F. C. L. Crespi, M. Cromaz, G. de Angelis, J. Eberth, P. Fallon, E. Farnea, E. Fioretto, S. J. Freeman, A. Gadea, K. Geibel, W. Gelletly, A. Gengelbach, A. Giaz, A. Gørgen, A. Gottardo, A. B. Hayes, H. Hess, H. Hua, P. R. John, J. Jolie, A. Jungclaus, W. Korten, I. Y. Lee, S. Leoni, X. Liang, S. Lunardi, A. O. Macchiavelli, R. Menegazzo, D. Mengoni, C. Michelagnoli, T. Mijatović, G. Montagnoli, D. Montanari, D. Napoli, C. J. Pearson, L. Pellegrini, Zs. Podolyák, G. Pollarolo, A. Pulia, F. Radeck, F. Recchia, P. H. Regan, E. Şahin, F. Scarlassara, G. Sletten, J. F. Smith, P.-A. Söderström, A. M. Stefanini, T. Steinbach, O. Stezowski, S. Szilner, B. Szpak, R. Teng, C. Ur, V. Vandone, D. Ward, D. D. Warner, A. Wiens, and C. Y. Wu, “High-spin structure of ^{134}Xe ,” *Phys. Rev. C* **93**, 054325 (2016).
- [10] P. J. Rothschild, A. M. Baxter, S. M. Burnett, M. P. Fewell, G. J. Gyapong, and R. H. Spear, “Quadrupole moment of the first excited state of ^{136}Ba ,” *Phys. Rev. C* **34**, 732–735 (1986).

- [11] M. Ohshima, S. Hayashibe, N. Kawamura, Y. Itoh, M. Fujioka, and T. Ishimatsu, “Magnetic moment of the 2140.2 keV 5^- state in ^{136}Ba ,” *Hyperfine Interactions* **7**, 103–107 (1979).
- [12] W. Gelletly, J. A. Moragues, M. A. J. Mariscotti, and W. R. Kane, “ $^{135}\text{Ba}(n, \gamma)$ reaction and level structure of ^{136}Ba ,” *Phys. Rev.* **181**, 1682–1696 (1969).
- [13] E. Dragulescu, G. Semenescu, and I. Iftimia, “Nuclear structure studies of nuclei near $N = 80$,” *J. Phys.* **53**, 447–451 (1999).
- [14] T. Shizuma, Z. G. Gan, K. Ogawa, H. Nakada, M. Ohshima, Y. Toh, T. Hayakawa, Y. Hatsukawa, M. Sugawara, Y. Utsuno, and Z. Liu, “A new isomer in ^{136}Ba populated by deep inelastic collisions,” *Eur. Phys. J. A* **20**, 207–210 (2004).
- [15] T. Bhattacharjee, S. Chanda, S. Bhattacharyya, S.K. Basu, R.K. Bhowmik, J.J. Das, U. Datta Pramanik, S.S. Ghugre, N. Madhavan, A. Mukherjee, G. Mukherjee, S. Muralithar, and R.P. Singh, “Band structures in near spherical ^{138}Ce ,” *Nuc. Phys. A* **825**, 16 – 38 (2009).
- [16] C. M. Petrache, M. Fantuzzi, G. LoBianco, D. Mengoni, A. Neusser-Neffgen, H. Hübel, A. Al-Khatib, P. Bringel, A. Bürger, N. Nenoff, G. Schönwasser, A. K. Singh, I. Ragnarsson, G. B. Hagemann, B. Herskind, D. R. Jensen, G. Sletten, P. Fallon, A. Görgen, P. Bednarczyk, D. Curien, G. Gangopadhyay, A. Korichi, A. Lopez-Martens, B. V. T. Rao, T. S. Reddy, and Nirmal Singh, “Evolution from spherical single-particle structure to stable triaxiality at high spins in ^{140}Nd ,” *Phys. Rev. C* **72**, 064318 (2005).
- [17] J. C. Merdinger, F. A. Beck, E. Bozek, T. Byrski, C. Gehringer, Y. Schutz, and J. P. Vivien, “Magnetic moments of the $I^\pi = 10^+$ isomers in Ce and Nd $N = 80$ isotones,” *Nucl. Phys. A* **346**, 281 – 284 (1980).
- [18] E. Gülmez, H. Li, and J. A. Cizewski, “Level structure of ^{140}Nd ,” *Phys. Rev. C* **36**, 2371–2379 (1987).
- [19] C. M. Petrache, R. A. Bark, S. T. H. Murray, M. Fantuzzi, E. A. Lawrie, S. Lang, J. J. Lawrie, S. M. Maliage, D. Mengoni, S. M. Mullins, S. S. Ntshangase, D. Petrache, T. M. Ramashidzha, and I. Ragnarsson, “Six-quasiparticle isomer in ^{140}Nd ,” *Phys. Rev. C* **74**, 034304 (2006).
- [20] M. Ferraton, R. Bourgain, C. M. Petrache, D. Verney, F. Ibrahim, N. de Séréville, S. Franchoo, M. Lebois, C. Phan Viet, L. Sagui, I. Stefan, J. F. Clavelin, and M. Vilmay, “Lifetime measurement of the six-quasiparticle isomer in ^{140}Nd and evidence for an isomer above the $19/2^+$ state in ^{139}Nd ,” *Eur. Phys. J. A* **35**, 167–170 (2008).
- [21] “Evaluated Nuclear Structure Data File (ENSDF),” <http://www.nndc.bnl.gov/ensdf>.
- [22] A. Vogt, B. Birkenbach, P. Reiter, A. Blazhev, M. Siciliano, K. Hadyńska-Klęk, J. J. Valiente-Dobón, C. Wheldon, E. Teruya, N. Yoshinaga, K. Arnsward, D. Bazzacco, M. Bowry, A. Bracco, B. Bruyneel, R. S. Chakrawarthy, R. Chapman, D. Cline, L. Corradi, F. C. L. Crespi, M. Cromaz, G. de Angelis, J. Eberth, P. Fallon, E. Farnea, E. Fioretto, S. J. Freeman, B. Fu, A. Gadea, K. Geibel, W. Gelletly, A. Gengelbach, A. Giaz, A. Görgen, A. Gottardo, A. B. Hayes, H. Hess, R. Hirsch, H. Hua, P. R. John, J. Jolie, A. Jungclaus, L. Kaya, W. Korten, I. Y. Lee, S. Leoni, L. Lewandowski, X. Liang, S. Lunardi, A. O. Macchiavelli, R. Menegazzo, D. Mengoni, C. Michelagnoli, T. Mijatović, G. Montagnoli, D. Montanari, C. Müller-Gatermann, D. Napoli, C. J. Pearson, L. Pellegrini, Zs. Podolyák, G. Pollarolo, A. Pullia, M. Queiser, F. Radeck, F. Recchia, P. H. Regan, D. Rosiak, N. Saed-Samii, E. Şahin, F. Scarlasara, D. Schneiders, M. Seidlitz, B. Siebeck, G. Sletten, J. F. Smith, P.-A. Söderström, A. M. Stefanini, T. Steinbach, O. Stezowski, S. Szilner, B. Szpak, R. Teng, C. Ur, V. Vandone, D. D. Warner, A. Wiens, C. Y. Wu, and K. O. Zell, “Isomers and high-spin structures in the $N = 81$ isotones ^{135}Xe and ^{137}Ba ,” *Phys. Rev. C* **95**, 024316 (2017).
- [23] A. Kerek and J. Kownacki, “The level structure of the $N = 81$ and 82 nucleides $^{137,138}\text{Ba}$ as investigated in $^{136}\text{Xe}(\alpha, xn)$ reactions,” *Nucl. Phys. A* **206**, 245 – 272 (1973).
- [24] S. Kaim, C. M. Petrache, A. Gargano, N. Itaco, T. Zerrouki, R. Leguillon, A. Astier, I. Deloncle, T. Konstantinopoulos, J. M. Régis, D. Wilmsen, B. Melon, A. Nannini, C. Ducoin, D. Guinet, and T. Bhattacharjee, “High-spin spectroscopy of ^{139}Ce ,” *Phys. Rev. C* **91**, 024318 (2015).
- [25] P. Bhattacharyya, P. J. Daly, C. T. Zhang, Z. W. Grabowski, S. K. Saha, B. Fornal, R. Broda, W. Urban, I. Ahmad, D. Seweryniak, I. Wiedenhöver, M. P. Carpenter, R. V. F. Janssens, T. L. Khoo, T. Lauritsen, C. J. Lister, P. Reiter, and J. Blomqvist, “Yrast excitations in $n = 81$ nuclei ^{132}Sb and ^{133}Te from ^{248}Cm fission,” *Phys. Rev. C* **64**, 054312 (2001).
- [26] J. K. Hwang, A. V. Ramayya, J. H. Hamilton, C. J. Beyer, J. O. Rasmussen, Y. X. Luo, S. C. Wu, T. N. Ginter, C. M. Folden, P. Fallon, P. M. Zielinski, K. E. Gregorich, A. O. Macchiavelli, M. Stoyer, S. J. Asztalos, A. Covello, and A. Gargano, “Particle-hole excited states in ^{133}Te ,” *Phys. Rev. C* **65**, 034319 (2002).
- [27] Yu. Khazov, A. Rodionov, and F. G. Kondev, “Nuclear data sheets for $A = 133$,” *Nucl. Data Sheets* **112**, 855 – 1113 (2011).
- [28] B. K. Wagner, P. E. Garrett, Minfang Yeh, and S. W. Yates, “On the first excited state of ^{137}Ba ,” *J. Radioanal. Nucl. Chem.* **219**, 217–220 (1997).
- [29] I. Bikit, I. Aničin, J. Slivka, M. Krmar, J. Puzović, and Lj. Čonkić, “Population of the 283 keV level of ^{137}Ba by the β decay of ^{137}Cs ,” *Phys. Rev. C* **54**, 3270–3272 (1996).
- [30] V. A. Bondarenko, I. L. Kuvaga, P. T. Prokofjev, A. M. Sukhovojev, V. A. Khitrov, Yu. P. Popov, S. Brant, and V. Paar, “Levels of ^{137}Ba studied with neutron-induced reactions,” *Nucl. Phys. A* **582**, 1 – 22 (1995).
- [31] E. Dragulescu, M. Ivascu, R. Mihu, D. Popescu, G. Semenescu, A. Velenik, and V. Paar, “Coulomb excitation of levels in ^{135}Ba and ^{137}Ba ,” *J. Phys. G* **10**, 1099 (1984).
- [32] A. Kerek and J. Kownacki, “The level structure of the $N = 81$ and 82 nucleides $^{137,138}\text{Ba}$ as investigated in $^{136}\text{Xe}(\alpha, xn)$ reactions,” *Nucl. Phys. A* **206**, 245 – 272 (1973).
- [33] Somen Chanda, Tumpa Bhattacharjee, Sarmishtha Bhattacharyya, Anjali Mukherjee, Swapan Kumar Basu, I. Ragnarsson, R. K. Bhowmik, S. Muralithar, R. P. Singh, S. S. Ghugre, and U. Datta Pramanik, “Seven-quasiparticle bands in ^{139}Ce ,” *Phys. Rev. C* **79**, 054332 (2009).
- [34] D. Bucurescu, G. Căta-Danil, I. Căta-Danil, M. Ivaşcu, N. Mărginean, R. Mărginean, L. C. Mihăilescu, C. Rusu, and G. Suliman, “Gamma-ray spectroscopy of the nu-

- cleus ^{139}Ce ,” *Eur. Phys. J. A* **27**, 301–312 (2006).
- [35] S. Bhowal, C. Lahiri, R. Raut, P. Singh, M. K. Raju, A. Goswami, A. K. Singh, S. Bhattacharya, T. Bhattacharjee, G. Mukherjee, *et al.*, “Energy levels in ^{141}Nd from fusion evaporation study,” *J. Phys. G* **38**, 035105 (2011).
- [36] T. Zerrouki, C. M. Petrache, R. Leguillon, K. Hauschild, A. Korichi, A. Lopez Martens, S. Frauendorf, I. Ragnarsson, H. Hübel, A. Neußer-Neffgen, A. nd Al-Khatib, P. Bringel, A. Bürger, N. Nenoff, G. Schönwaßer, A. K. Singh, D. Curien, G. B. Hagemann, B. Herskind, G. Sletten, P. Fallon, A. Görgen, and P. Bednarczyk, “Shape evolution and magnetic rotation in ^{141}Nd ,” *Eur. Phys. J. A* **51**, 50 (2015).
- [37] S. Akkoyun *et al.*, “AGATA – Advanced GAMMA Tracking Array,” *Nucl. Instrum. Methods Phys. Res. A* **668**, 26 (2012).
- [38] A. M. Stefanini, L. Corradi, G. Maron, A. Pisent, M. Trotta, A. M. Vinodkumar, S. Beghini, G. Montagnoli, F. Scarlassara, G. F. Segato, A. De Rosa, G. Inghima, D. Pierroutsakou, M. Romoli, M. Sandoli, G. Pollarolo, and A. Latina, “The heavy-ion magnetic spectrometer PRISMA,” *Nucl. Phys. A* **701**, 217 – 221 (2002).
- [39] L. Corradi, S. Szilner, G. Pollarolo, D. Montanari, E. Fioretto, A. M. Stefanini, J. M. Valiente-Dobón, E. Farnea, C. Michelagnoli, G. Montagnoli, F. Scarlassara, C. A. Ur, T. Mijatović, D. Jelavić Malenica, N. Soić, and F. Haas, “Multinucleon transfer reactions: Present status and perspectives,” *Nucl. Instrum. Methods Phys. Res. B* **317**, Part B, 743 – 751 (2013).
- [40] S. Szilner, C. A. Ur, L. Corradi, N. Marginean, G. Pollarolo, A. M. Stefanini, S. Beghini, B. R. Behera, E. Fioretto, A. Gadea, B. Guiot, A. Latina, P. Mason, G. Montagnoli, F. Scarlassara, M. Trotta, G. de Angelis, F. Della Vedova, E. Farnea, F. Haas, S. Lenzi, S. Lunardi, R. Marginean, R. Menegazzo, D. R. Napoli, M. Nespolo, I. V. Pokrovsky, F. Recchia, M. Romoli, M.-D. Salsac, N. Soić, and J. J. Valiente-Dobón, “Multinucleon transfer reactions in closed-shell nuclei,” *Phys. Rev. C* **76**, 024604 (2007).
- [41] L. Netterdon, V. Derya, J. Endres, C. Fransen, A. Hennig, J. Mayer, C. Müller-Gatermann, A. Sauerwein, P. Scholz, M. Spieker, and A. Zilges, “The γ -ray spectrometer HORUS and its applications for nuclear astrophysics,” *Nucl. Instrum. Methods Phys. Res. A* **754**, 94 – 100 (2014).
- [42] A. Gadea, E. Farnea, J. J. Valiente-Dobón, B. Million, D. Mengoni, D. Bazzacco, F. Recchia, A. Dewald, Th. Pissulla, W. Rother, G. de Angelis, *et al.*, “Conceptual design and infrastructure for the installation of the first AGATA sub-array at LNL,” *Nucl. Instrum. Methods Phys. Res. A* **654**, 88 – 96 (2011).
- [43] A. Wiens, H. Hess, B. Birkenbach, B. Bruyneel, J. Eberth, D. Lersch, G. Pascovici, P. Reiter, and H.-G. Thomas, “The AGATA triple cluster detector,” *Nucl. Instrum. Methods Phys. Res. A* **618**, 223 – 233 (2010).
- [44] B. Bruyneel, B. Birkenbach, and P. Reiter, “Pulse shape analysis and position determination in segmented HPGe detectors: The AGATA detector library,” *Eur. Phys. J. A* **52**, 70 (2016).
- [45] A. Lopez-Martens, K. Hauschild, A. Korichi, J. Roccaz, and J.-P. Thibaud, “ γ -ray tracking algorithms: a comparison,” *Nucl. Instrum. Methods Phys. Res. A* **533**, 454 – 466 (2004).
- [46] A. Vogt, B. Birkenbach, P. Reiter, L. Corradi, T. Mijatović, D. Montanari, S. Szilner, D. Bazzacco, M. Bowry, A. Bracco, B. Bruyneel, F. C. L. Crespi, G. de Angelis, P. Désesquelles, J. Eberth, E. Farnea, E. Fioretto, A. Gadea, K. Geibel, A. Gengelbach, A. Giaz, A. Görgen, A. Gottardo, J. Grebosz, H. Hess, P. R. John, J. Jolie, D. S. Judson, A. Jungclaus, W. Korten, S. Leoni, S. Lunardi, R. Menegazzo, D. Mengoni, C. Michelagnoli, G. Montagnoli, D. Napoli, L. Pellegrini, G. Pollarolo, A. Pullia, B. Quintana, F. Radeck, F. Recchia, D. Rosso, E. Şahin, M. D. Salsac, F. Scarlassara, P.-A. Söderström, A. M. Stefanini, T. Steinbach, O. Stezowski, B. Szpak, Ch. Theisen, C. Ur, J. J. Valiente-Dobón, V. Vandone, and A. Wiens, “Light and heavy transfer products in $^{136}\text{Xe}+^{238}\text{U}$ multinucleon transfer reactions,” *Phys. Rev. C* **92**, 024619 (2015).
- [47] N. Saed-Samii, Diplomarbeit, Universität zu Köln (2013), unpublished.
- [48] J. Theuerkauf, *Die Analyse von zwei- und mehrdimensionalen $\gamma\gamma$ -Koinzidenzspektren an Beispielen aus Hochspinexperimenten in der Massengegend um ^{146}Gd* , Ph.D. thesis, Universität zu Köln (1994).
- [49] I. Wiedenhöver, “Computer code CORLEONE,” (1997), unpublished.
- [50] I. Wiedenhöver, O. Vogel, H. Klein, A. Dewald, P. von Brentano, J. Gableske, R. Krücken, N. Nicolay, A. Gelberg, P. Petkov, A. Gizon, J. Gizon, D. Bazzacco, C. Rossi Alvarez, G. de Angelis, S. Lunardi, P. Pavan, D. R. Napoli, S. Frauendorf, F. Dönau, R. V. F. Janssens, and M. P. Carpenter, “Detailed angular correlation analysis with 4π spectrometers: Spin determinations and multipolarity mixing measurements in ^{128}Ba ,” *Phys. Rev. C* **58**, 721–728 (1998).
- [51] K. S. Krane and R. M. Steffen, “Determination of the $E2/M1$ Multipole Mixing Ratios of the Gamma Transitions in ^{110}Cd ,” *Phys. Rev. C* **2**, 724–734 (1970).
- [52] K. S. Krane, R. M. Steffen, and R. M. Wheeler, “Directional correlations of gamma radiations emitted from nuclear states oriented by nuclear reactions or cryogenic methods,” *At. Data Nucl. Data Tables* **11**, 351 – 406 (1973).
- [53] A. Linnemann, *Das HORUS-Würfelspektrometer und Multiphononanregungen in ^{106}Cd* , Ph.D. thesis, Universität zu Köln (2006).
- [54] L. Bettermann, C. Fransen, S. Heinze, J. Jolie, A. Linnemann, D. Mücher, W. Rother, T. Ahn, A. Costin, N. Pietralla, and Y. Luo, “Candidates for the one-phonon mixed-symmetry state in ^{130}Xe ,” *Phys. Rev. C* **79**, 034315 (2009).
- [55] S. Kumar, A. K. Jain, Alpana Goel, S. S. Malik, R. Palit, H. C. Jain, I. Mazumdar, P. K. Joshi, Z. Naik, A. Dhal, T. Trivedi, I. Mehrotra, S. Appannababu, L. Chaturvedi, V. Kumar, R. Kumar, D. Negi, R. P. Singh, S. Muralithar, R. K. Bhowmik, and S. C. Pancholi, “Band structure and shape coexistence in $^{135}\text{Ba}_{79}$,” *Phys. Rev. C* **81**, 067304 (2010).
- [56] S. Chanda, T. Bhattacharjee, S. Bhattacharyya, S. K. Basu, R. K. Bhowmik, S. Muralithar, R.P. Singh, B. Mukherjee, N.S. Pattabiraman, S.S. Ghugre, and M. B. Chatterjee, “High spin spectroscopy of ^{137}La ,” *Nucl. Phys. A* **775**, 153 – 174 (2006).
- [57] T. Yamazaki, “Tables of coefficients for angular distribution of gamma rays from aligned nuclei,” *Nucl. Data, Sect. A* **3**, 1 – 23 (1967).

- 1477 [58] Y. Khazov, A. A. Roionpv, S. Sakharov, and B. Singh, 1541
 1478 “Nuclear data sheets for $A = 132$,” *Nucl. Data Sheets* 1542
 1479 **104**, 497 (2005). 1543
- 1480 [59] M. Kortelahti, A. Pakkanen, M. Piiparinen, T. Komppa, 1544
 1481 and R. Komu, “Medium-spin levels and a 360 ns $I^\pi = 19/2^-$ 1545
 1482 isomer in the $N = 80$ nucleus ^{137}La ,” *Nucl Phys.* 1546
 1483 **A 376**, 245–272 (1982). 1547
- 1484 [60] B. A. Brown and W. D. M. Rae, “The Shell-Model Code 1541
 1485 NuShellX@MSU,” *Nucl. Data Sheets* **120**, 115 – 118 1542
 1486 (2014).
- 1487 [61] N. Shimizu, “Nuclear shell-model code for massive paral- 1541
 1488 lel computation, “KSHELL”,” (2013), [arXiv:1310.5431](https://arxiv.org/abs/1310.5431) 1542
 1489 [[nucl-ph](https://arxiv.org/abs/1310.5431)].
- 1490 [62] E. Caurier, G. Martínez-Pinedo, F. Nowacki, A. Poves, 1541
 1491 and A. P. Zuker, “The shell model as a unified view of 1542
 1492 nuclear structure,” *Rev. Mod. Phys.* **77**, 427–488 (2005).
- 1493 [63] E. Caurier, F. Nowacki, A. Poves, and K. Sieja, “Collec- 1541
 1494 tivity in the light xenon isotopes: A shell model study,” 1542
 1495 *Phys. Rev. C* **82**, 064304 (2010).
- 1496 [64] E. Caurier, F. Nowacki, and A. Poves, “Shell Model 1541
 1497 description of the $\beta\beta$ decay of ^{136}Xe ,” *Phys. Lett. B* **711**, 1542
 1498 **62 – 64** (2012).
- 1499 [65] R. Machleidt, F. Sammarruca, and Y. Song, “Nonlocal 1541
 1500 nature of the nuclear force and its impact on nuclear 1542
 1501 structure,” *Phys. Rev. C* **53**, R1483–R1487 (1996).
- 1502 [66] L. Coraggio, A. Covello, A. Gargano, N. Itaco, and 1541
 1503 T.T.S. Kuo, “Effective shell-model hamiltonians from real- 1542
 1504 istic nucleon-nucleon potentials within a perturbative 1543
 1505 approach,” *Annals of Physics* **327**, 2125 – 2151 (2012).
- 1506 [67] L. Coraggio, A. Covello, A. Gargano, N. Itaco, and 1541
 1507 T.T.S. Kuo, “Shell-model calculations and realistic effec- 1542
 1508 tive interactions,” *Progress in Particle and Nuclear* 1543
 1509 *Physics* **62**, 135 – 182 (2009).
- 1510 [68] L. Coraggio, L. De Angelis, T. Fukui, A. Gargano, and 1541
 1511 N. Itaco, “Calculation of gamow-teller and two-neutrino 1542
 1512 double- β decay properties for ^{130}Te and ^{136}Xe with a 1543
 1513 realistic nucleon-nucleon potential,” *Phys. Rev. C* **95**, 1544
 1514 **064324** (2017).
- 1515 [69] E. Teruya, N. Yoshinaga, K. Higashiyama, and A. Oda- 1541
 1516 hara, “Shell-model calculations of nuclei around mass 1542
 1517 130,” *Phys. Rev. C* **92**, 034320 (2015).
- 1518 [70] K. Higashiyama and N. Yoshinaga, “Pair-truncated shell- 1541
 1519 model analysis of nuclei around mass 130,” *Phys. Rev. C* 1542
 1520 **83**, 034321 (2011).
- 1521 [71] B. A. Brown, N. J. Stone, J. R. Stone, I. S. Towner, and 1541
 1522 M. Hjorth-Jensen, “Magnetic moments of the 2_1^+ states 1542
 1523 around ^{132}Sn ,” *Phys. Rev. C* **71**, 044317 (2005).
- 1524 [72] L. Kaya, A. Vogt, P. Reiter, M. Siciliano, B. Birken- 1541
 1525 bach, A. Blazhev, L. Coraggio, E. Teruya, N. Yoshinaga, 1542
 1526 K. Higashiyama, K. Arnsward, D. Bazzacco, A. Bracco, 1543
 1527 B. Bruyneel, L. Corradi, F. C. L. Crespi, G. de Ange- 1544
 1528 lis, J. Eberth, E. Farnea, E. Fioretto, C. Fransen, B. Fu, 1545
 1529 A. Gadea, A. Gargano, A. Giaz, A. Gørgen, A. Gottardo, 1546
 1530 K. Hadyńska-Klęk, H. Hess, R. Hetzenegger, R. Hirsch, 1547
 1531 N. Itaco, P. R. John, J. Jolie, A. Jungclaus, W. Korten, 1548
 1532 S. Leoni, L. Lewandowski, S. Lunardi, R. Menegazzo, 1549
 1533 D. Mengoni, C. Michelagnoli, T. Mijatović, G. Montag- 1550
 1534 noli, D. Montanari, C. Müller-Gatermann, D. Napoli, Zs. 1551
 1535 Podolyák, G. Pollarolo, A. Pullia, M. Queiser, F. Rec- 1552
 1536 chia, D. Rosiak, N. Saed-Samii, E. Şahin, F. Scarlassara, 1553
 1537 D. Schneiders, M. Seidlitz, B. Siebeck, J. F. Smith, P.- 1554
 1538 A. Söderström, A. M. Stefanini, T. Steinbach, O. Ste- 1555
 1539 zowski, S. Szilner, B. Szpak, C. Ur, J. J. Valiente-Dobón, 1556
 1540 K. Wolf, and K. O. Zell, “High-spin structure in the tran- 1557
 sitional nucleus ^{131}Xe : Competitive neutron and proton 1558
 alignment in the vicinity of the $n = 82$ shell closure,” 1559
Phys. Rev. C **98**, 014309 (2018). 1560
- [73] Y. Utsuno, T. Otsuka, N. Shimizu, M. Honma, 1541
 T. Mizusaki, Y. Tsunoda, and T. Abe, “Recent shell- 1542
 model results for exotic nuclei,” *EPJ Web of Conferences* 1543
66, 02106 (2014).